Mon. Not. R. Astron. Soc. 000, 000–000 (0000) Printed 20 June 2014 (MN LaTeX style file v2.2)

The ATLAS^{3D} project – XXVII. Cold Gas and the Colours and Ages of Early-type Galaxies

Lisa M. Young[1,2⋆], Nicholas Scott[3], Paolo Serra[4,5], Katherine Alatalo[6], Estelle Bayet[7], Leo Blitz[8], Maxime Bois[9], Frédéric Bournaud[10], Martin Bureau[7], Alison F. Crocker[11], Michele Cappellari[7], Roger L. Davies[7], Timothy A. Davis[12], P. T. de Zeeuw[12,13], Pierre-Alain Duc[10], Eric Emsellem[12,14], Sadegh Khochfar[15], Davor Krajnović[16], Harald Kuntschner[12], Richard M. McDermid[17,18,19], Raffaella Morganti[4,20], Thorsten Naab[21], Tom Oosterloo[4,20], Marc Sarzi[22], and Anne-Marie Weijmans[23]

[1]*Physics Department, New Mexico Institute of Mining and Technology, Socorro, NM 87801, USA*
[2]*Academia Sinica Institute of Astronomy & Astrophysics, PO Box 23-141, Taipei 10617, Taiwan, R.O.C.*
[3]*Sydney Institue for Astronomy (SIfA), School of Physics, The University of Sydney, NSW 2006, Australia*
[4]*Netherlands Institute for Radio Astronomy (ASTRON), Postbus 2, 7990 AA Dwingeloo, The Netherlands*
[5]*CSIRO Astronomy and Space Science, Australia Telescope National Facility, PO Box 76, Epping, NSW 1710, Australia*
[6]*Infrared Processing and Analysis Center, California Institute of Technology, Pasadena, California 91125, USA*
[7]*Sub-Dept. of Astrophysics, Dept. of Physics, University of Oxford, Denys Wilkinson Building, Keble Road, Oxford, OX1 3RH, UK*
[8]*Department of Astronomy, Hearst Field Annex, University of California, Berkeley, CA 94720, USA*
[9]*Observatoire de Paris, LERMA and CNRS, 61 Av. de l'Observatoire, F-75014 Paris, France*
[10]*Laboratoire AIM Paris-Saclay, CEA/IRFU/SAp – CNRS – Université Paris Diderot, 91191 Gif-sur-Yvette Cedex, France*
[11]*Ritter Astrophysical Observatory, University of Toledo, Toledo, OH 43606, USA*
[12]*European Southern Observatory, Karl-Schwarzschild-Str. 2, 85748 Garching, Germany*
[13]*Sterrewacht Leiden, Leiden University, Postbus 9513, 2300 RA Leiden, the Netherlands*
[14]*Université Lyon 1, Observatoire de Lyon, Centre de Recherche Astrophysique de Lyon and Ecole Normale Supérieure de Lyon, 9 avenue Charles André, F-69230 Saint-Genis Laval, France*
[15]*Royal Observatory Edinburgh, Blackford Hill, Edinburgh, EH9 3HJ, UK*
[16]*Leibniz-Institut für Astrophysik Potsdam (AIP), An der Sternwarte 16, D-14482 Potsdam, Germany*
[17]*Australian Astronomical Observatory, PO Box 296, Epping, NSW 1710, Australia*
[18]*Department of Physics and Astronomy, Macquarie University, NSW 2109, Australia*
[19]*Gemini Observatory, Northern Operations Centre, 670 N. A'ohoku Place, Hilo, HI 96720, USA*
[20]*Kapteyn Astronomical Institute, University of Groningen, Postbus 800, 9700 AV Groningen, The Netherlands*
[21]*Max-Planck-Institut für Astrophysik, Karl-Schwarzschild-Str. 1, 85741 Garching, Germany*
[22]*Centre for Astrophysics Research, University of Hertfordshire, Hatfield, Herts AL1 9AB, UK*
[23]*School of Physics and Astronomy, University of St Andrews, North Haugh, St Andrews KY16 9SS, UK*

20 June 2014

ABSTRACT

We present a study of the cold gas contents of the ATLAS^{3D} early-type galaxies, in the context of their optical colours, near-UV colours, and Hβ absorption line strengths. Early-type (elliptical and lenticular) galaxies are not as gas-poor as previously thought, and at least 40% of local early-type galaxies are now known to contain molecular and/or atomic gas. This cold gas offers the opportunity to study recent galaxy evolution through the processes of cold gas acquisition, consumption (star formation), and removal. Molecular and atomic gas detection rates range from 10% to 34% in red sequence early-type galaxies, depending on how the red sequence is defined, and from 50% to 70% in blue early-type galaxies. Notably, massive red sequence early-type galaxies (stellar masses $> 5\times10^{10}$ M$_\odot$, derived from dynamical models) are found to have H I masses up to M(H I)/M$_\star \sim 0.06$ and H$_2$ masses up to M(H$_2$)/M$_\star \sim 0.01$. Some 20% of all massive early-type galaxies may have retained atomic and/or molecular gas through their transition to the red sequence. However, kinematic and metallicity signatures of external gas accretion (either from satellite galaxies or the intergalactic medium) are also common, particularly at stellar masses $\leqslant 5 \times 10^{10}$ M$_\odot$, where such signatures are found in $\sim 50\%$ of H$_2$-rich early-type galaxies. Our data are thus consistent with a scenario in which fast rotator early-type galaxies are quenched former spiral galaxies which have undergone some bulge growth processes, and in addition, some of them also experience cold gas accretion which can initiate a period of modest star formation activity. We discuss implications for the interpretation of colour-magnitude diagrams.

Key words: galaxies: elliptical and lenticular, cD — galaxies: evolution — galaxies: ISM — galaxies: structure — Radio lines: galaxies.

1 INTRODUCTION

While early-type (elliptical and lenticular) galaxies generally have smaller relative amounts of star formation activity than spirals, they are not all completely devoid of such activity. Modest rates of star formation in early-type galaxies can be traced with UV colours, mid-IR and far-IR continuum emission, mid-IR PAH emission, optical emission lines, and cm-wave radio continuum emission (e.g. Shapiro et al. 2010; Sarzi et al. 2010). Surveys of UV and optical colours have suggested that this kind of low-level star formation activity is present in around a quarter of all nearby early-type galaxies (Yi et al. 2005; Kaviraj et al. 2007; Suh et al. 2010). Recently Smith et al. (2012) have emphasized that star formation can be found even in early-type galaxies which are on the red sequence, and Fumagalli et al. (2013) have measured star formation rates in optically quiescent galaxies out to redshifts of 1–2.

This evidence for star formation activity should be understood in the context of paradigms for the development of the red sequence. Star formation requires cold gas, and the treatment of cold gas is a crucial element of galaxy evolution models. For example, one class of models assumes that the development of the red sequence is driven by AGN activity, as AGN-driven outflows remove the star-forming gas from blue gas-rich galaxies (eg. Kaviraj et al. 2011). The outflow is assumed to remove the gas more quickly than it could be consumed by star formation activity. Cold gas may also be removed or consumed by a variety of other processes associated with bulge growth (Cheung et al. 2012). Another class of models points out that it may not be necessary to *remove* the cold gas, but simply to sterilize it (Kawata et al. 2007; Martig et al. 2009, 2013). In order to test these paradigms for the development of the red sequence, and in particular to test the relative importance of gas recycling, accretion and removal as galaxies move to and from the red sequence, we explore the relationships between the colours of early-type galaxies, their Hβ absorption line strengths, and their cold gas content.

There have been several other surveys for molecular gas in various samples of early-type galaxies (e.g. Welch, Sage & Young 2010), but the ATLAS^{3D} project is the only one which also has the kinematic information that is necessary to interpret galaxies' recent evolutionary histories. Stellar kinematics, shells and tidal features give insight into the merger and assembly histories of the galaxies, and ionized gas, H I, and molecular kinematics reveal signs of gas accretion and/or gravitational disturbances. Thus, the ATLAS^{3D} project is the first opportunity to bring together the evidence from star formation activity (recorded in the colours and Hβ absorption of the stellar populations) and the recent interaction/accretion history recorded in the gas. In this paper we do not deal with measurements of an instantaneous star formation rate or star formation efficiencies derived therefrom (e.g. Martig et al. 2013). Instead, we focus particularly on the connections between gas accretion and the star formation history over the last few Gyr, as those are encoded in the stellar populations.

Section 2 of this paper describes the ATLAS^{3D} sample of local early-type galaxies. Section 3 gives explanatory information on the provenance of the colour, stellar population, and cold gas data. Section 4 shows the atomic and molecular gas contents of early-type galaxies, both on and off the red sequence. Depending on which colours are used to define the red sequence, 10%±2% to 34%±6% of red sequence early-type galaxies have $> 10^7$ M$_\odot$ of cold gas. A discussion of internal extinction is found in Section 5, which shows that although the H$_2$-rich galaxies are dusty, the dust usually has only modest effects on integrated colours. Section 6 compiles multiple types of evidence for recent gas accretion and finds no systematic difference in the colours or stellar populations of galaxies with and without such evidence. A "frosting" or rejuvenation model that invokes a small quantity of recent star formation on a red sequence galaxy can explain the colours and Hβ absorption line strengths of the H$_2$-rich ATLAS^{3D} early-type galaxies. Section 7 notes some differences between the high (stellar) mass H$_2$ detections and their low (stellar) mass counterparts. Section 8 summarizes the conclusions of the work.

2 SAMPLE

The ATLAS^{3D} early-type galaxy sample is a complete volume-limited sample of galaxies brighter than $M_K = -21.5$, covering distances out to 42 Mpc, with some restrictions on Declination and Galactic latitude (see Cappellari et al. 2011a, hereafter Paper I). The early-type sample is actually drawn from a parent sample which has no colour or morphological selection, and optical images of the entire parent sample have been inspected by eye for large-scale spiral structure. The 260 galaxies lacking spiral structure form the basis of the ATLAS^{3D} project; integral-field optical spectroscopy over a field of at least 33″× 41″ was obtained with the SAURON instrument (Bacon et al. 2001) on the William Herschel Telescope for these 260 galaxies. Paper I also tabulates their assumed distances and foreground optical extinctions.

The ATLAS^{3D} early-type galaxies clearly trace out the optical red sequence, and they also include a smaller population of somewhat bluer galaxies (Paper I). Detailed study of the stellar kinematic maps is used to reveal internal substructures such as counter-rotating stellar cores or kinematically decoupled stellar discs (Krajnović et al. 2011, Paper II). The specific angular momenta of the galaxies are analyzed in Emsellem et al. (2011) (Paper III) in the context of formation paradigms for slow and fast rotators (Bois et al. 2011; Khochfar et al. 2011; Naab et al. 2013). Dynamical masses are provided by Cappellari et al. (2013a,b). Other work on the sample probes environmental drivers of galaxy evolution (Cappellari et al. 2011b; Cappellari 2013), hot gas (Sarzi et al. 2013), stellar populations and star formation histories (McDermid et al. 2013), and bulge/disc decompositions (Krajnović et al. 2013).

3 DATA

3.1 Cold gas, line strengths and stellar population ages

All of the ATLAS^{3D} early-type galaxies except NGC 4486A were observed with the IRAM 30m telescope in the ^{12}CO J=1-0 and 2-1 lines (Young et al. 2011, Paper IV).[1] The CO detection limits correspond to H$_2$ masses of approximately 10^7 M$_\odot$ for the nearest galaxies and 10^8 M$_\odot$ for the more distant galaxies. To place this CO survey in context it is crucial to note that the luminosity selection criterion for the sample is based purely on the total K_S-band stellar luminosity, not the FIR flux or even the B luminosity (which have been used in the past, and which are strongly influenced by the presence of star formation). The CO detection rate is 22%±3%; detected H$_2$ masses range from $10^{7.1}$ to $10^{9.3}$ M$_\odot$ and the molecular/stellar mass ratios M(H$_2$)/M$_\star$ range from 3.4×10^{-4} to 0.076.

[1] NGC 4486A was missed because the velocity information in NED and HyperLEDA was inaccurate at the time of the obervations.

In addition, the CO detection rate and M(H_2)/$M_\star$ distributions are broadly consistent between Virgo Cluster and field galaxies, so that the cluster environment has not strongly affected the molecular gas content.

The brightest CO detections in the SAURON sample (de Zeeuw et al. 2002) were mapped in CO J=1-0 emission with the BIMA and Plateau de Bure millimeter interferometers, giving the molecular gas distribution and kinematics at typically 5″ resolution (Young 2002, 2005; Young, Bureau & Cappellari 2008; Crocker et al. 2008, 2009a, 2011). Similarly, the brightest CO detections in the remainder of the ATLAS^{3D} sample were mapped with CARMA for this project (Alatalo et al. 2013a). These CO maps have been obtained for a total of 40 ATLAS^{3D} galaxies, which is by far the largest and most robustly defined currently available sample of molecular gas maps of early-type galaxies. The molecular gas is found in kpc-scale structures (Davis et al. 2013a), often in discs or rings, and these data provide kinematic information for our discussion of the galaxies' histories and their location/movement in the colour-magnitude diagram.

Observations of H I are available for all of the ATLAS^{3D} early-type galaxies at declinations $> 10°$, except the four closest in projection to M87 (Serra et al. 2012). The H I detection rate is 32%±4%, and H I mass upper limits range from 2.9×10^6 $M_\odot$ to 3.8×10^7 $M_\odot$. Detected H I masses fall in roughly the same range as the molecular masses, i.e. M(H I)/$M_\star = 10^{-4}$ to 10^{-1}. These interferometric observations are made with the Westerbork Synthesis Radio Telescope (WSRT), covering $\sim 30'$ fields of view at typical resolutions of $35''\times 45''$. The data thus allow us to consider both the total H I content of the galaxy and to isolate the portion of atomic gas which is located (in projection) in the central regions of the galaxy, in an area comparable to the SAURON field of view and about three times larger than the beam of the 30m telescope. The difference between the total and central H I measurements can be significant because, as Oosterloo et al. (2010) and Serra et al. (2012) have noted, the H I distributions occasionally extend to more than 10 effective radii; furthermore, H I is sometimes only detected in the outskirts of a galaxy. As we will show, the central H I detections are much better correlated with molecular gas than are the total H I detections. The central H I masses are presented in Table 1.

McDermid et al. (2013) present Hβ absorption line strength measurements for the ATLAS^{3D} galaxies, along with the best-fit single or simple stellar population (SSP) ages and metallicities. As discussed by Trager et al. (2000) and Kuntschner et al. (2010), for example, the SSP parameters can be thought of as luminosity-weighted mean stellar properties, although the weight bias of the SSP ages towards young populations is even stronger than their luminosities would suggest (Serra & Trager 2007). The measurements are made in circular apertures of radius R_e (the galaxy's effective or half-light radius), $R_e/2$, and $R_e/8$. Here we make use of the $R_e/2$ apertures, on the grounds that they are most similar to the size of the IRAM 30m beam, and the $R_e/8$ apertures, which are the most sensitive to small amounts of recent star formation activity near the galaxy centers.

3.2 Optical and UV photometry

The Sloan Digital Sky Survey (SDSS) u and r magnitudes and foreground extinctions for ATLAS^{3D} galaxies are obtained from Data Release 8 (DR8, Aihara et al. 2011). The matched-aperture 'modelMag' magnitudes are used to compute colours and the Petrosian r magnitude is used for an absolute magnitude M_r. For five bright galaxies we were unable to find object matches of any type, primary or secondary, in DR8, even though primary matches are identified in DR7; for these five the DR7 magnitudes are used. They are NGC numbers 3608, 4374, 4459, 4486, and 4649. Some caution is required in these cases. Aihara et al. (2011) note that the DR8 photometry was computed with an updated sky measurement algorithm, and the update tends to make extended galaxies brighter. Indeed, a comparison of DR7 and DR8 photometry for the ATLAS^{3D} galaxies suggests that objects of $r \leqslant 12$ are about 0.5 mag brighter in DR8 than in DR7. Thus the DR7 photometry of the 'missing' galaxies is manually adjusted 0.5 mag brighter to make the values commensurate with DR8 photometry. The offset between DR8 and DR7 is roughly uniform in all filters and therefore does not distort colours as much as luminosities. Blanton et al. (2011) and Scott et al. (2013) have further shown that the DR8 catalog photometry still underestimates the fluxes of extended galaxies by 0.5 mag or more, but Blanton et al. (2011) have again demonstrated that the effect on colours is minimal.

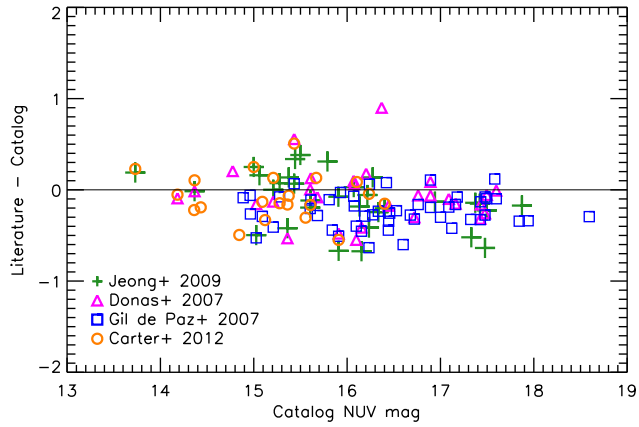

Figure 1. Comparison of previously published NUV magnitudes and GALEX catalog GR7 data for the ATLAS^{3D} sample. The pink triangle outlier is NGC 4578, for which the new catalog data use a deeper exposure than Donas et al. (2007) used.

Near-UV magnitudes for the ATLAS^{3D} galaxies were obtained from the GALEX catalog server, release GR7. They are corrected for foreground extinction assuming the Milky Way $E(B-V)$ values from Schlegel et al. (1998), just as for the SDSS data above, and scaled to NUV as $A_{NUV} = 8.0 * E(B-V)$ (Gil de Paz et al. 2007). One quarter of the ATLAS^{3D} galaxies have additional published NUV photometry derived from extrapolation to curves of growth or from two-dimensional image fits, and Figure 1 presents a comparison of the catalog photometry to the results of Donas et al. (2007), Gil de Paz et al. (2007), Jeong et al. (2009), and Carter et al. (2011). There may be a systematic offset on the order of 0.2 mag for faint galaxies (NUV $\geqslant$ 16), in the sense that the published magnitudes are brighter than the catalog values.

We use the asymptotic NUV magnitudes and the 2MASS K_S-band magnitudes (Jarrett et al. 2000) to compute NUV−K colours. While this procedure is not as accurate as aperture matching, it is adequate for our purposes here as we use the photometry only to indicate the distributions of galaxies within a colour-magnitude diagram. Likewise any systematic offsets on the order of 0.2 mag are still small compared to the scatter in the colours of red sequence galaxies.

Table 1. Central H I masses

Name		log M(H I)/$M_\odot$	Name		log M(H I)/$M_\odot$	Name		log M(H I)/$M_\odot$
IC0598	<	7.06	NGC3674	<	7.02	NGC4649	<	7.19
IC3631	<	7.34	NGC3694	<	7.11	NGC4660	<	6.50
NGC0661	<	6.99	NGC3757	<	6.72	NGC4694	=	7.13 (0.02)
NGC0680	=	7.65 (0.05)	NGC3796	<	6.72	NGC4710	=	6.71 (0.08)
NGC0770	<	7.17	NGC3838	<	7.23	NGC4733	<	7.12
NGC0821	<	6.53	NGC3941	<	6.17	NGC4754	<	7.18
NGC1023	=	6.84 (0.02)	NGC3945	<	6.73	NGC4762	<	7.41
NGC2481	<	7.03	NGC3998	=	7.42 (0.02)	NGC5103	=	7.30 (0.04)
NGC2549	<	6.12	NGC4026	<	7.14	NGC5173	=	8.45 (0.01)
NGC2577	<	6.96	NGC4036	<	6.80	NGC5198	<	6.98
NGC2592	<	6.80	NGC4078	<	7.26	NGC5273	<	6.42
NGC2594	<	7.22	NGC4111	=	6.94 (0.04)	NGC5308	<	7.24
NGC2679	<	6.97	NGC4119	<	7.10	NGC5322	<	6.96
NGC2685	=	7.36 (0.02)	NGC4143	<	6.42	NGC5342	<	7.12
NGC2764	=	8.91 (0.01)	NGC4150	=	6.04 (0.06)	NGC5353	<	7.07
NGC2768	<	6.61	NGC4168	<	7.08	NGC5355	<	7.11
NGC2778	<	6.68	NGC4203	=	7.03 (0.03)	NGC5358	<	7.13
NGC2824	=	7.45 (0.08)	NGC4251	<	6.58	NGC5379	<	6.97
NGC2852	<	6.90	NGC4262	<	7.02	NGC5422	=	7.43 (0.05)
NGC2859	<	6.85	NGC4267	<	7.17	NGC5473	<	7.02
NGC2880	<	6.65	NGC4278	=	6.06 (0.09)	NGC5475	<	6.89
NGC2950	<	6.31	NGC4283	<	5.97	NGC5481	<	6.83
NGC3032	=	7.80 (0.01)	NGC4340	<	6.65	NGC5485	<	6.79
NGC3073	=	8.01 (0.02)	NGC4346	<	6.27	NGC5500	<	6.97
NGC3098	<	6.73	NGC4350	<	6.50	NGC5557	<	7.16
NGC3182	=	6.93 (0.16)	NGC4371	<	7.10	NGC5582	<	6.88
NGC3193	<	7.07	NGC4374	<	6.88	NGC5611	<	6.76
NGC3226	<	6.72	NGC4377	<	7.16	NGC5631	=	7.54 (0.03)
NGC3230	<	7.33	NGC4379	<	7.04	NGC5687	<	6.94
NGC3245	<	6.61	NGC4382	<	6.59	NGC5866	=	6.67 (0.06)
NGC3248	<	6.84	NGC4387	<	6.65	NGC6149	<	7.18
NGC3301	<	6.75	NGC4406	<	6.40	NGC6278	<	7.28
NGC3377	<	6.14	NGC4425	<	6.33	NGC6547	<	7.25
NGC3379	<	6.11	NGC4429	<	7.12	NGC6548	<	6.74
NGC3384	<	6.19	NGC4435	<	7.23	NGC6703	<	6.80
NGC3400	<	6.81	NGC4452	<	7.27	NGC6798	=	8.10 (0.02)
NGC3412	<	6.17	NGC4458	<	6.53	NGC7280	=	7.25 (0.05)
NGC3414	<	7.70	NGC4459	<	6.53	NGC7332	<	6.70
NGC3457	=	6.95 (0.07)	NGC4461	<	7.33	NGC7454	<	6.78
NGC3458	<	6.97	NGC4473	<	6.47	NGC7457	<	6.22
NGC3489	=	6.53 (0.03)	NGC4474	<	7.09	NGC7465	=	8.64 (0.01)
NGC3499	=	6.77 (0.14)	NGC4477	<	6.56	PGC028887	<	7.29
NGC3522	<	7.48	NGC4489	<	6.35	PGC029321	<	7.30
NGC3530	<	6.98	NGC4494	<	6.46	PGC035754	<	7.20
NGC3595	<	7.04	NGC4503	<	7.15	PGC044433	<	7.28
NGC3599	<	6.64	NGC4521	<	7.18	PGC050395	<	7.13
NGC3605	<	6.44	NGC4528	<	7.19	PGC051753	<	7.13
NGC3607	<	6.53	NGC4550	<	6.50	PGC061468	<	7.15
NGC3608	<	6.53	NGC4551	<	7.39	PGC071531	<	6.98
NGC3610	<	6.63	NGC4552	<	6.48	UGC03960	=	7.06 (0.11)
NGC3613	<	6.90	NGC4564	<	6.53	UGC04551	<	6.87
NGC3619	=	8.25 (0.01)	NGC4596	<	7.13	UGC05408	=	8.33 (0.02)
NGC3626	=	7.80 (0.02)	NGC4608	<	7.22	UGC06176	=	8.40 (0.02)
NGC3648	<	6.99	NGC4621	<	6.48	UGC08876	<	7.05
NGC3658	<	7.04	NGC4638	<	7.13	UGC09519	=	7.75 (0.02)
NGC3665	<	7.05						

Notes: Central H I fluxes are those observed within one WSRT resolution element centred on the optical nucleus (for additional description see Oosterloo et al. 2010). We attempt to account for beam smearing effects in that the cases with poorly resolved central H I holes are treated as upper limits. The upper limits are calculated as a 3σ uncertainty on a sum over one beam and 50 km s^{-1}; that strategy is motivated by Serra et al. (2012). Uncertainties on H I masses are quoted as 1σ on a sum over one beam and 50 km s^{-1}, with a 3% absolute calibration uncertainty added in quadrature.

3.3 Stellar masses

Two different estimates of stellar mass are used in this paper. One, denoted $M_\star$, is derived from K_S luminosities using $M_{K\odot} = 3.28$ (Binney & Tremaine 2008) and a typical stellar mass-to-light ratio of $M_\star/L_K = 0.82$ in solar units (Bell et al. 2003). The other, denoted $M_{\rm JAM}$ and used more frequently, is a dynamical mass derived from self-consistent modeling of the stellar kinematics and the isophotal structure of each galaxy (Cappellari et al. 2013a). It can be understood as $M_{\rm JAM} \approx 2 \times M_{1/2}$, where $M_{1/2}$ is the total mass within a sphere enclosing half of the galaxy light. Given that the proportion of dark matter is small inside that sphere, $M_{\rm JAM}$ approximates a stellar mass that also accounts for systematic variations in the initial mass function (Cappellari et al. 2013b). The derivation of $M_{\rm JAM}$ assumes that the stellar mass-to-light ratio is spatially constant within a galaxy, but unlike the case of $M_\star$, it does not assume the ratio is the same for all galaxies. Trends in the stellar mass-to-light ratios are discussed in Cappellari et al. (2013b). For our purposes here, we note that the two measures of stellar mass are nearly linearly correlated with the median value of $\log(M_{\rm JAM}/M_\star)$ being 0.17 dex and the dispersion being 0.15 dex.

4 COLD GAS IN RED SEQUENCE GALAXIES

4.1 Molecular gas

Figures 2 through 5 show colour-magnitude diagrams and their analogs for the ATLAS^{3D} early-type galaxies, with symbol sizes scaled to the molecular gas masses. Figure 2 presents $u-r$ colours and Figure 3 shows NUV−K colours with the modification that molecular masses are normalized to the stellar mass as $M(H_2)/M_\star$. A comparison of the two panels provides visual illustration of important statistical results from Figure 7 of Paper IV, namely that the CO detection rate and $M(H_2)$ distributions are surprisingly constant over the luminosity range of the sample. Thus in Figure 3 there is a trend for $M(H_2)/M_\star$ to be larger for low luminosity galaxies, but statistically speaking it is because $M_\star$ is smaller and not because $M(H_2)$ is larger. Cappellari et al. (2013b) have also shown that, at fixed stellar mass, galaxies with low stellar velocity dispersion and large effective radius have larger molecular masses; in other words, molecular gas in early-type galaxies is preferentially associated with a discy stellar component. The masses of the stellar discs in question are much larger than the currently observable molecular masses, though, as suggested by the $M(H_2)/M_\star$ values in Figure 3.

The red sequence is clearly evident in these figures, as are a number of the ATLAS^{3D} members in the green valley and even into the blue cloud. These 'blue tail' early-type galaxies are found in the lower mass portion of the sample, with $M_r > -20.5$, $M_K > -23.4$ or $\log(M_{\rm JAM}/M_\odot) < 10.7$; according to the luminosity functions derived by Bell et al. (2003) they have $L \leqslant 0.6L^*$. Galaxies with higher masses are still on the red sequence. The 'blue tail' early-type galaxies are therefore analogous to those detected in clusters at moderate redshift, for example, by Jaffé et al. (2011). The CO detection rate is 0.54 ± 0.06 to 0.70 ± 0.08 among them, depending on which colours are used to define the blue tail. (More extensive discussion of cold gas detection rates will be found in section 4.3.) They have the highest values of $M(H_2)/M_{\rm JAM}$ in the sample, namely 0.01 to 0.07, and those values are comparable to the typical spiral galaxies in the COLD GASS sample (Kauffmann et al. 2013). These facts support the suggestion that the blue tail galaxies are blue because of ongoing star formation.

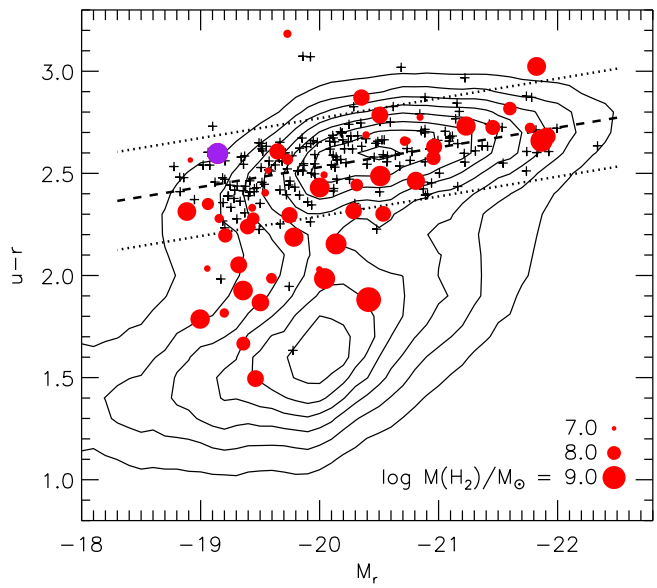

Figure 2. Optical colour-magnitude diagram for the ATLAS^{3D} sample. CO detections are marked with red circles and nondetections with black crosses; the sizes of the red circles indicate the value of $M(H_2)$, scaled logarithmically as indicated in the legend. Contours underneath show the red sequence and the blue cloud as demarcated by a sample of 60000 galaxies with redshifts in the range $0.01 \leqslant z \leqslant 0.08$ from SDSS Data Release 8. No $V/V_{\rm max}$ correction is applied, so the contours are intended to mark the general locations of the red sequence and the blue cloud in this diagram but not to indicate relative numbers of galaxies in different regions. The dashed line is the red sequence ridgeline and the dotted ones are parallel lines 2σ redder and bluer, as described in section 4.3. The purple symbol is UGC 09519, which is discussed in the text along with NGC 1266 as examples of galaxies with red colours but strong Hβ absorption. NGC 1266 does not appear in this plot because it is outside the SDSS coverage area.

They are also known to have younger stellar populations in their centers (Scott et al. 2013; Kuntschner et al. 2010). The relatively few CO-nondetected blue tail galaxies tend to be at large distances, $D \geqslant 35$ Mpc, so we suspect their molecular gas contents are just below our sensitivity limits. In contrast to the blue tail galaxies, many of the CO detections, particularly those with $L \geqslant 0.6L^*$ or $\log(M_{\rm JAM}/M_\odot) > 10.7$, also belong to galaxies which are located in the heart of the optical and UV–NIR red sequence.

Figure 4 presents an analog of a colour-magnitude diagram, constructed using the Hβ absorption line strength index (interior to $R_e/2$) in the role of colour. The dynamical mass $M_{\rm JAM}$ is used in place of a stellar luminosity. As both the Hβ line strength and NUV−K colour are sensitive to the presence of young stellar populations, and as the ATLAS^{3D} sample displays a tight relationship between Hβ line strength and NUV−K colour, Figures 3 and 4 are qualitatively similar. The only notable differences are two outliers in the (NUV−K) – Hβ relation, NGC 1266 and UGC 09519, which are both red sequence galaxies in NUV−K colours but have strong Hβ absorption. They might be experiencing a recent shutdown in star formation activity, as an abrupt shutdown would show up in the NUV flux before the Hβ line strength (see also Alatalo et al. 2013b). These galaxies are also known to have internal reddening from dust, and colour images are presented in Alatalo et al. (2013a).

Even more so than the NUV−K diagram, the Hβ-mass diagram dramatically emphasizes a dichotomy between a tight red

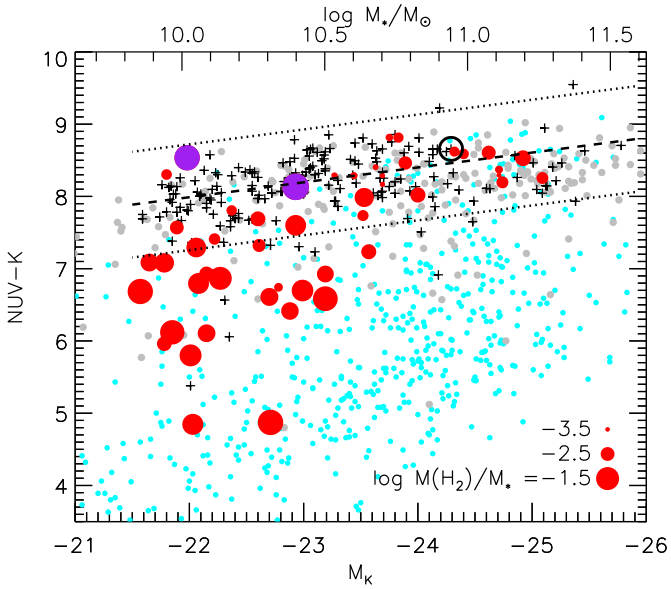

Figure 3. NUV−K colour-magnitude diagram with H_2 masses. Symbols and dotted lines are as in Figure 2. For context, cyan and grey dots are from the GALEX UV Atlas of Nearby Galaxies (Gil de Paz et al. 2007), where cyan dots are late type galaxies (morphological type $T \geqslant 0$) and grey dots are early types ($T < 0$). Note that the NUV magnitudes are measured in the AB system whereas the K_S magnitudes are in the Vega system. Since the ATLAS^{3D} GALEX data are taken from the GALEX pipeline catalog, and Figure 1 shows a median offset of 0.19 mag between the pipeline and the NUV magnitudes of Gil de Paz et al. (2007), the data from that paper have been shifted to account for the relative offset. Purple symbols mark NGC 1266 and UGC 09519, which are discussed in the text; NGC 1266 is the higher luminosity one of the pair. NGC 4552, a well-known UV upturn galaxy, is circled in black to demonstrate that the effects of the UV upturn are comparable to the dispersion in red sequence colours.

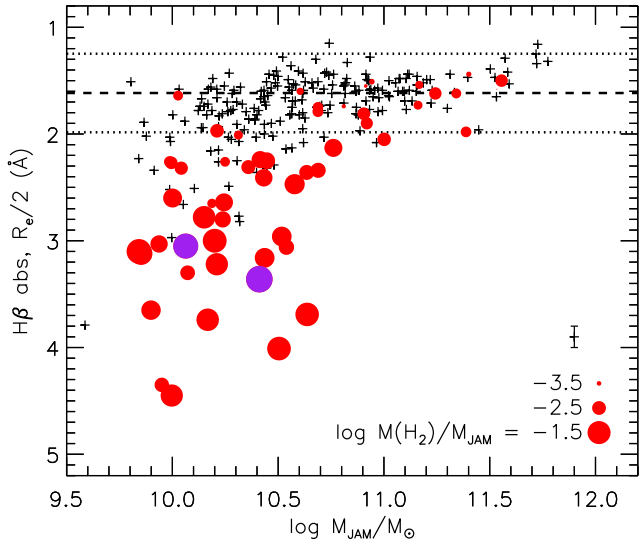

Figure 4. Hβ absorption line strength vs. stellar mass M_{JAM}, with H_2 masses. Symbols and lines are as for Figures 2 and 3; purple symbols again are NGC1266 and UGC09519. The mean uncertainty in the Hβ line strength is 0.1 Å (McDermid et al. 2013), and it is indicated in the lower right corner with an error bar showing $\pm 1\sigma$.

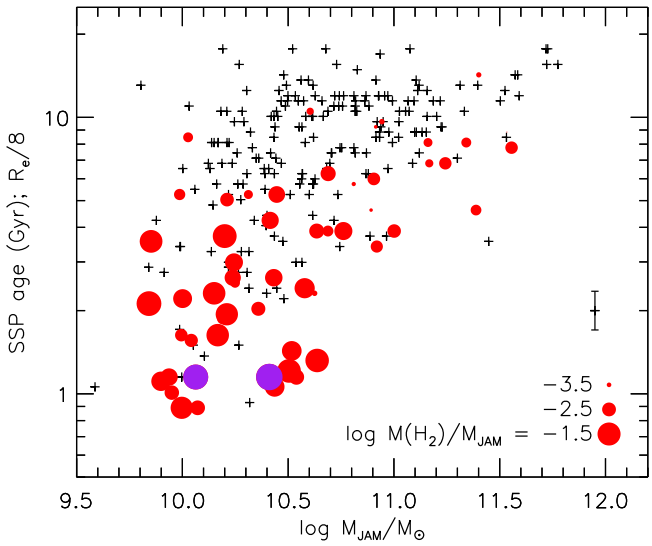

Figure 5. "Colour-magnitude" diagram using the inferred stellar SSP ages in place of colours and dynamical masses M_{JAM} in place of absolute magnitude. NGC 1266 and UGC 09519 are again shown in purple. The uncertainties in the SSP ages range from Δ(log age) = 0.04 dex to 0.12 dex, with a mean of 0.07 dex (McDermid et al. 2013), and that uncertainty is shown in the lower right corner with an errorbar of ± 0.07 dex.

sequence at high stellar masses and a large dispersion in Hβ absorption line strengths at lower stellar masses. The demarcation line, at around $\log(M_{JAM}/M_{\odot}) = 10.7$, also marks changes in the structural properties of the ATLAS^{3D} galaxies. Above that mass, the galaxies tend to be spheroid-dominated systems. Below that mass, early-type galaxies include both spheroid-dominated and disc-dominated systems with a wide range of velocity dispersions and effective radii. The disc-dominated systems have more molecular gas and younger stellar populations than the spheroid-dominated systems (Cappellari et al. 2013b).

Figure 5 involves the highest degree of analysis and interpretation, as its axes are constructed from the dynamical mass M_{JAM} and the SSP age (McDermid et al. 2013). Here we have used the SSP age measured in a central aperture of radius $R_e/8$ (typically only a couple of arcseconds) and we observe that the smaller apertures are more sensitive to recent star formation activity than large apertures (see also McDermid et al. 2013). For example, the CO-detected galaxies with $M_{JAM} > 10^{11}$ $M_{\odot}$ do not exhibit enhanced Hβ absorption in an $R_e/2$ aperture (Figure 4), but they do exhibit younger ages in an $R_e/8$ aperture. While the trend remains for a smaller age dispersion at higher masses, it is not such a sharp disparity as in NUV−K colours and Hβ line strength.

Figures 2 through 5 give a different perspective on the H_2 content of early-type galaxies than the CO searches of the COLD GASS project (Saintonge et al. 2011). That paper finds no CO emission in any red sequence galaxy, but its CO observations were not as deep and its sensitivity limits would miss most of the detections in the ATLAS^{3D} sample. The stellar mass range covered by both samples is very similar. However, only 8 of the 56 CO detections in the ATLAS^{3D} sample would simultaneously meet the stellar mass and CO sensitivity criteria of Saintonge et al. (2011), and only two of those (NGC 1266 and UGC 09519) are on the red sequence

in NUV−K and $u-r$ colours. A stacking analysis of the COLD GASS data is presented in Saintonge et al. (2012), but stacking removes all information about which individual galaxies have gas. The improvements in sensitivity of the ATLAS^{3D} project pick up significant numbers of molecular gas detections in red sequence early-type galaxies. Extreme examples of these red sequence galaxies with small but nonzero molecular masses can also be found in the detections of shocked H_2 emission in radio galaxies (Ogle et al. 2010).

4.2 Atomic gas

The ATLAS^{3D} sample displays a broad range of H_2/H I mass ratios, with measured values from 10^2 to 10^{-2} (see also Welch, Sage & Young 2010). Figure 6 presents the age-mass diagram with H_2, total H I and central H I masses. When considering the total H I contents, the distribution of H I-rich galaxies is markedly different from that of the H_2-rich galaxies. For example, only 8 of 56 H_2-rich galaxies (0.14±0.05) have SSP ages $\geqslant$ 8 Gyr; however, 19 of 53 H I-rich galaxies (0.36±0.07) have such large ages. For space considerations we have not shown H I contents on the optical, NUV or Hβ-magnitude diagrams, but the same effect is present there and is even stronger at dynamical masses $\log(M_{\rm JAM}/M_\odot) < 10.5$. Interestingly, H_2 is primarily detected in fast rotators (Young et al. 2011) whereas H I is detected in both fast and slow rotators (Serra et al. 2013), so the slow rotators are more commonly H I-rich than H_2-rich.

When considering only the central H I masses, however (Figure 6, lower panel), we find that the galaxies with central H I detections have age and mass distributions indistinguishable from those of the H_2 detections. The central H I masses are comparable to or smaller than the H_2 masses, as already noted by Oosterloo et al. (2010) and Serra et al. (2012), and this is undoubtedly due to the fact that the atomic column densities are smaller than the molecular column densities in the galaxy centers (Blitz & Rosolowsky 2006; Leroy et al. 2008; Lucero & Young 2013). The one known exception with a large (central H I)/H_2 mass ratio $\sim 3.1 \pm 0.6$ is NGC 3073, and in the absence of a CO map for the galaxy we can only speculate that its CO emission may be distributed over a smaller area than its H I.

These data strengthen the suggestions of Morganti et al. (2006), Serra et al. (2008), and Oosterloo et al. (2010) that the extended atomic gas reservoirs in early-type galaxies are not necessarily associated with recent star formation activity as traced in the galaxies' integrated colours, Hβ absorption line strength indices, or SSP ages. As Serra et al. (2012) have noted, the H I column densities in early-type galaxies tend to be smaller than those in spirals. Atomic gas may be associated with star formation activity in an extended UV-bright disc, as in Thilker et al (2010), but more careful surveys of GALEX data and deep optical imaging (e.g. Duc et al. 2011) should be conducted to assess this activity in the ATLAS^{3D} sample.

In summary, molecular gas and *central* atomic gas in early-type galaxies are almost always associated with recent star formation activity which can be seen in the SSP ages, particularly at small radii. For early-type galaxies with $\log(M_{\rm JAM}/M_\odot) < 10.7$, the recent star formation activity manifests itself also in the Hβ line strength and NUV−K, but often it is not noticeable in integrated $u-r$ colours. For the highest mass early-type galaxies the star formation activity is not detectable in either optical or UV–NIR integrated colours.

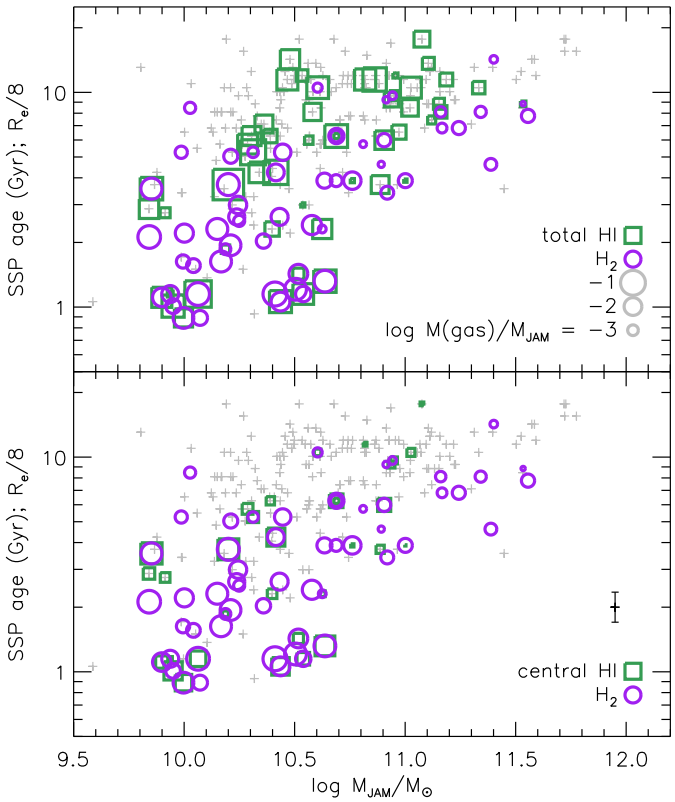

Figure 6. Atomic gas (Serra et al. 2012) and molecular gas in the age-mass diagram. As in the previous figure, the errorbar in the lower right corner shows a typical uncertainty in the SSP age. Gray crosses are CO nondetections; cold gas contents are indicated by the sizes of the green squares (H I) and purple circles (H_2). The top panel shows the total H I content associated with the galaxy, whereas the bottom panel shows only the H I content within the central WSRT synthesized beam ($\sim 30'' - 40''$ diameter, roughly comparable to the $22''$ aperture used for CO measurements). The H_2/H I mass ratios can also be inferred from the symbol sizes; a galaxy with H_2/H I = 1 has a concentric circle and square of the same diameter. In comparing atomic and molecular masses, it is worthwhile to remember that some of the H_2 detections lack H I data due to the Declination limit on the WSRT observations. However, all of the H I detections do have CO measurements.

4.3 Implications of cold gas in red sequence galaxies

To quantify the cold gas content in red sequence early-type galaxies, we first make an empirical definition of the red sequence in ATLAS^{3D}. We fit lines to the colours and Hβ absorption line strengths of all galaxies not detected in CO emission; these lines define the ridgelines of the red sequence. In the case of Hβ absorption the fitted line is constrained to have no slope. The dispersions characterizing the width of the red sequence are estimated by fitting Gaussians to the histograms of residuals (again using only CO nondetections). Such a Gaussian fit is more robust to outliers than simply computing the standard deviation directly. Galaxies within 2σ of the ridgeline, or redder, are defined to be red sequence galaxies. Figures 2 through 4 show the red sequence ridgelines and the blue edges defined in this manner. Table 2 gives the red sequence parameters and Table 3 gives the detection rates for cold gas in red sequence galaxies. In the ATLAS^{3D} sample the galaxies with $\log(M_{\rm JAM}/M_\odot) > 10.7$ or $L > 0.6L^*$ are red sequence galaxies,

Table 2. Red Sequence Definitions

"Colour"	Ridgeline	σ
$u-r$	$u-r=0.59-0.097(M_r)$	0.12 mag
NUV−K	NUV−K$=3.83-0.187(M_K)$	0.37 mag
Hβ $(R_e/2)$	H$\beta=1.62$ Å	0.18 Å

with very few exceptions, and therefore detection statistics for the high-mass galaxies are also given.

We note, first, that the detection rates of cold gas in early-type red sequence galaxies are still substantial. For example, in H_2 they range from 10% (using Hβ to define the red sequence) to 16% ($u-r$), and in total H I content they are 24% (using Hβ) to 34% (high-mass galaxies). This result is qualitatively consistent with the detection rate of dust through far-IR emission from red sequence early-type galaxies (Smith et al. 2012). When low-mass early-type galaxies are detected in cold gas emission, they tend to be blue; however, when high-mass early-type galaxies are similarly detected, they are still on the red sequence. Thus, for red sequence early-type galaxies, the cold gas detection rates are higher among the more massive galaxies than among the low-mass galaxies. The effect can be seen by comparing rows 5 and 6 in Table 3. Detection rates of (total) atomic gas are also always higher in red sequence galaxies than detection rates of molecular gas. In the ATLAS^{3D} sample the red sequence early-type galaxies have total H I masses up to 5×10^9 $M_\odot$, central H I masses up to 2.5×10^8 $M_\odot$ and H_2 masses up to 2×10^9 $M_\odot$. Those latter two maximum values depend at a factor of two level on the indicator (colour or Hβ index) used to define the red sequence. Normalized to stellar masses, the red sequence galaxies have total ratios M(H I)/M_{JAM} $\leqslant 0.16$, central M(H I)/M_{JAM} $\leqslant 0.01$ and M(H_2)/M_{JAM} $\leqslant 0.07$.

At high stellar masses, the red sequence is just as well-defined for galaxies rich in cold gas as for galaxies poor in cold gas. Specifically, the Kolmogorov-Smirnov and Mann-Whitney U tests show no statistically significant differences in the integrated colours or Hβ absorption strengths of the high-mass CO detections and non-detections, or the H I detections and nondetections. The aperture must be restricted to very small sizes (e.g. $R_e/8$, as in Figure 5) before enhanced Hβ values become measurable in H_2-rich massive galaxies.

Colour-magnitude relations are often used to study the quenching of star formation and the development of the red sequence (e.g. Snyder et al. 2012; Jaffé et al. 2011). Our data show that the approach to the red sequence may not necessarily involve the loss of all cold gas, even if one makes both colour *and* morphological cuts to select early-type galaxies. Thus it should not be assumed that gravitational interactions between such galaxies will always be dissipationless ('dry'; see also Chou, Bridge & Abraham 2012). Furthermore, at $z=0$ we observe that the presence of H_2 or H I does not increase colour scatter in $L>0.6L^*$ early-type galaxies. This result could have implications for the so-called scatter-age test (e.g. Jaffé et al. 2011), which uses colours to infer star formation activity in high luminosity galaxies. For the most massive ATLAS^{3D} galaxies, neither colours nor Hβ absorption line strengths identify H_2- or H I-rich galaxies, though for low luminosities the colours and Hβ can be partially successful at selecting gas-rich galaxies. Finally, if all galaxies' cold gas contents were generally higher in the past than they are now, our data at $z=0$ may provide only lower limits on the cold gas contents of red sequence galaxies at higher redshifts.

5 COLOUR CORRECTIONS FOR INTERNAL EXTINCTION

The previous section analyzed colour-magnitude relations using integrated colours without correction for internal dust reddening. Those uncorrected colours and their dispersions are appropriate for comparison to intermediate and high redshift studies of the red sequence (e.g. Snyder et al. 2012; Jaffé et al. 2011), where colours are also typically not corrected for internal dust. We now estimate how large such corrections would be.

Many different methods have been used to estimate the internal extinction in galaxies, including scaling from the far-IR thermal dust emission, the Balmer decrement, and/or the 4000 Å break, as well as from detailed fits of the spectra (e.g. Wyder et al. 2007; Schiminovich et al. 2007; Cortese, Gavazzi, & Boselli 2008; Gonçalves et al. 2012). But since early-type galaxies have smooth light distributions, and dust discs and filaments are readily visible in optical images of the ATLAS^{3D} galaxies (Krajnović et al. 2011; Scott et al. 2013; Alatalo et al. 2013a), we adopt the more straightforward method of measuring the internal extinction directly from optical images.

In Scott et al. (2013), $g-i$ colour maps are used to identify dusty regions and to de-redden those regions in r images. We allow for intrinsic colour gradients within galaxies by measuring the local $g-i$ colour excess from a linear trend in $g-i$ with radius (see Figure 2 of Scott et al. 2013). The resulting total internal extinctions A_r are measured as the difference in the integrated magnitude before and after the de-reddening correction, and are presented in Table 4. The corresponding extinctions for u, NUV, and K_S are calculated from a $R_V=3.1$ reddening law (Schlafly & Finkbeiner 2011) and, as above, $A_{NUV}=8.0E(B-V)$ (Gil de Paz et al. 2007). Measured total extinctions A_r range from 0.01 mag to 0.5 mag, with a median of 0.05 mag. For context and comparison, a dusty patch imposing 1 mag of extinction and covering 10% to 20% of an otherwise uniform source produces a total extinction of 0.067 to 0.139 mag.

Consistency checks on the extinctions in Table 4 can be made from the FIR luminosities of our sample galaxies. Specifically, following the prescription of Johnson et al. (2007), we compute the expected FUV extinction from the infrared excess IRX $=\log(L_{dust}/L_{UV})$. The justification of this method is that the FIR emission is reprocessed from UV emission intercepted by dust grains, so the FIR/UV ratio is a *de facto* measurement of the UV extinction. The expected FUV extinction can then be scaled back to A_r by our assumed reddening law. With one exception (NGC 2685, which has a dramatically bright FUV disc or ring), these predicted values of A_r are 3 to 20 times larger than the measured values of A_r. Indeed, this kind of a discrepancy between IR-derived and optically-derived dust masses has been known for many years (Goudfrooij & de Jong 1995), and it is not clear whether the IRX method can be applied in early-type galaxies in the same way as it is in spirals (Johnson et al. 2007). We therefore adopt the optically-derived extinctions and simply bear in mind that they may be underestimated, as they will tend to miss smoothly distributed dust components. FIR-based dust masses for many of the ATLAS^{3D} sample have also been presented by Smith et al. (2012), Martini, Dicken, & Storchi-Bergmann (2013), and Auld et al. (2013), among others; investigations of the dust properties are, however, beyond the scope of this paper.

Internal extinctions have not been measured for every galaxy in the ATLAS^{3D} sample. They have only been measured in cases where the de-reddened images were necessary for robust two-

Table 3. Cold Gas Detections in Early-Type Galaxies

Galaxy Subtype	Definition	CO data	H I data	Detection rates		
				H_2	Central H I	Total H I
(1)	(2)	(3)	(4)	(5)	(6)	(7)
all		259	166	22 (03)	19 (03)	32 (04)
$u-r$ red sequence	$u-r > 0.35 - 0.097(M_r)$	213	144	16 (02)	15 (03)	30 (04)
NUV−K red sequence	$NUV - K > 3.10 - 0.187(M_K)$	200	127	14 (03)	13 (03)	27 (04)
Hβ red sequence	H$\beta < 1.98$ Å	189	123	10 (02)	09 (03)	24 (04)
high mass ($\approx$ red sequence)	$\log(M_{\rm JAM}/M_\odot) > 10.7$	102	61	16 (04)	15 (04)	34 (06)
low-mass, Hβ red sequence	$\log(M_{\rm JAM}/M_\odot) \leqslant 10.7$ and H$\beta < 1.98$ Å	93	66	05 (02)	06 (03)	18 (05)
low-mass, Hβ 'blue tail'	$\log(M_{\rm JAM}/M_\odot) \leqslant 10.7$ and H$\beta \geqslant 1.98$ Å	64	39	55 (06)	49 (08)	51 (08)

Notes: Column 3 gives the total number of ATLAS^{3D} galaxies in each category that have CO data; this is the entire sample, minus NGC 4486A. Column 4 gives the number with H I data (Serra et al. 2012). The detection rates in columns 5–7 are percentages and include formal uncertainties in parentheses.

Table 4. Internal extinctions

Name	A_r (mag)	Name	A_r (mag)
IC1024	0.092	NGC4233	0.041
NGC2685	0.52	NGC4281	0.021
NGC2764	0.049	NGC4324	0.073
NGC3156	0.0038	NGC4429	0.22
NGC3489	0.012	NGC4459	0.014
NGC3499	0.092	NGC4476	0.013
NGC3607	0.016	NGC4526	0.16
NGC3619	0.051	NGC4753	0.052
NGC3626	0.024	NGC5379	0.048
NGC3665	0.031	NGC5631	0.0075
NGC4036	0.13	PGC056772	0.22
NGC4119	0.12	UGC06176	0.020

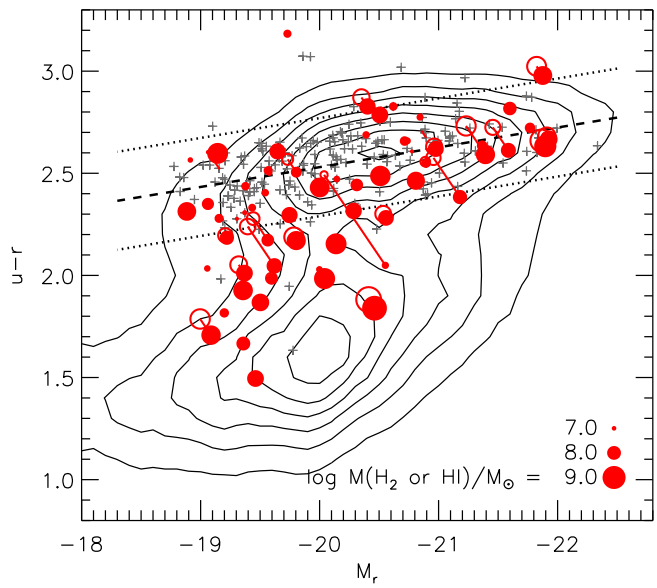

Figure 7. Similar to Figure 2, except that galaxies with central H I detections have been added, and corrections for internal extinction have been made for the galaxies in Table 4. Corrected photometry values (filled circles) are linked with a line to the values before correction (open circles).

dimensional image modelling in Scott et al. (2013). Hence some notable dusty galaxies are not represented in Table 4, either because the dust is spatially compact (e.g. UGC 09519 and NGC 1266), or a dust disc is nearly face-on (e.g. NGC 3032), or the dust is so optically thick that the de-reddening correction fails (e.g. NGC 4710 and NGC 5866). Nevertheless, the set with internal extinction data is an illustrative set of the gas-rich ATLAS^{3D} galaxies. Of the 24, 19 are detected in CO emission and an additional three are detected in H I emission (the remaining two have no H I data). Alatalo et al. (2013a), Crocker et al. (2011), and Young, Bendo & Lucero (2009) show some overlays of optical colour maps and CO integrated intensity distributions in the H_2-rich ATLAS^{3D} galaxies, to illustrate the close association of molecular gas and dust.

No internal extinction correction is attempted for the Hβ absorption index. In principle, as it is a narrow-baseline equivalent width measurement and the extinction will be approximately constant over a small wavelength range, Hβ is robust to a screen of dust. In practice, however, the Hβ line strengths could be underestimated (and the inferred SSP ages could be too old) if young stars are completely obscured behind dust clouds. Similarly, the colour correction measures colour excess with respect to the stellar populations surrounding the dust clouds or discs. If the stellar populations behind the dust clouds are younger, the broadband extinction corrections could be underestimated. This kind of an underestimate is probably a larger effect for the broadband colour than for the Hβ index as the stars dominating Hβ absorption are older and will have moved farther from their natal clouds.

Figures 7 and 8 are analogous to Figures 2 and 3, but the photometry has been corrected for internal extinction in those cases where such correction is available. This correction makes only modest alterations to the colour-magnitude diagrams. For example, in $u-r$, we find only four H_2-rich galaxies that are on the red sequence before correction and off the red sequence after correction (though, as mentioned above, NGC 1266, UGC 09519, NGC 4710, and NGC 5866 might also move off the red sequence with an internal extinction correction.) The highest mass, H_2-rich red sequence galaxies remain on the red sequence even with the extinction correction. We note also that the red sequence ridgelines and 2σ boundaries (Section 4.3) were defined using only CO-nondetected galaxies, so for practical purposes they are not affected by the internal extinction correction.

6 EVIDENCE FOR GAS ACCRETION

One possible interpretation of the cold gas detection rates in Table 3 is that early-type galaxies occasionally retain some atomic and/or

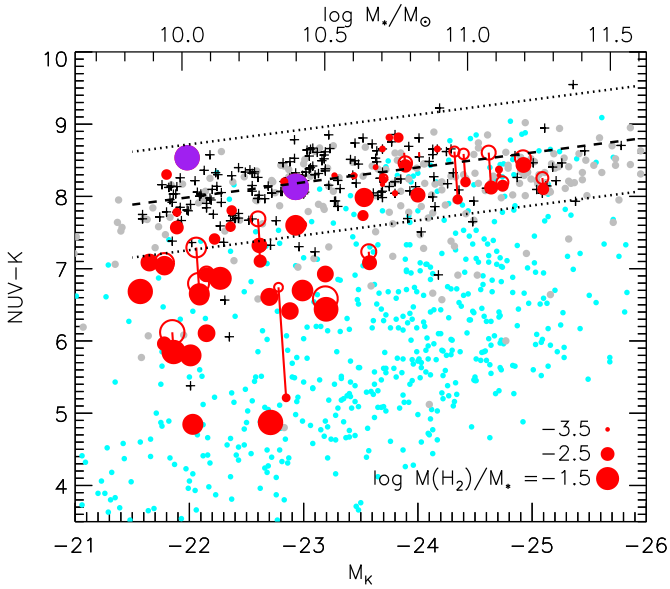

Figure 8. Similar to Figure 3, except that galaxies with central H I detections have been added, and corrections for internal extinction have been made for the galaxies in Table 4. Corrected photometry values (filled circles) are linked with a line to the values before correction (open circles).

molecular gas throughout their complex evolutionary histories, and through their transformations from late-type to early-type. Another is that they may have lost their original cold gas but acquired some new cold gas in recent times. As discussed by Davis et al. (2011) and McDermid et al. (2013), the kinematic and spectroscopic data of ATLAS^{3D} identify specific galaxies that have experienced recent gas accretion. The locations of these galaxies in the colour-magnitude diagrams can help to clarify which of the alternatives mentioned above may be more relevant to the development of the red sequence and the histories of the 'blue tail' early-type galaxies.

6.1 Identifying signatures of cold gas accretion or interactions

Kinematic misalignments between cold gas and stars indicate either that the gas was accreted, and its incoming orbital angular momentum was not parallel to the galaxy's angular momentum, or that the gas endured through some major disruption such as a merger. Thus the misalignments serve as markers of a galaxy's history. Kinematic misalignments can also occur if the galaxy's potential is significantly triaxial or barred. Triaxiality might be important for a few of the slow rotators in the sample, but it should not be important for most of the CO detections; a strong majority of them occur in fast rotators (Paper IV), and the fast rotators are consistent with being oblate (Krajnović et al. 2011; Emsellem et al. 2011; Weijmans et al. 2013; Cappellari et al. 2013b).

The kinematic misalignment angles between stars, molecular gas, and ionized gas are provided by Davis et al. (2011), who further show that the molecular gas kinematic position angles (PAs) are always consistent with ionized gas kinematic PAs where both can be measured. Similarly, misalignment angles between central H I and stellar kinematics are provided by Serra et al. (2013). Thus, galaxies are classified as having aligned gas or misaligned gas, with a dividing line at 30° which makes generous allowance for the uncertainties in PA measurement and for the presence of bars. Here we assume that all misaligned gas was accreted from some external source. This assumption will provide only a lower limit on the incidence of accreted gas, of course, as some of the aligned gas may also have been accreted.

McDermid et al. (2013) have also identified a subset of ATLAS^{3D} galaxies which exhibit unusually low stellar metallicities and strong α-element enhancement, when compared to their peers at similar stellar masses. The low metallicity/strong [α/Fe] stellar populations are concentrated in the centers of their host galaxies, and the hosts tend to be the most H_2-rich sample members in low-density environments. McDermid et al. (2013) propose that these galaxies have an underlying old stellar population which follows the same metallicity and α-element abundance trends as the rest of the sample, but they have accreted a substantial amount of low metallicity gas which has formed a younger and more metal-poor stellar population. The galaxies thus identified are IC 0676, IC 1024, NGC 2764, NGC 3073, NGC 4684, NGC 7465, PGC 056772, PGC 058114, PGC 061468, and UGC 05408, and in the following sections they are also treated as showing signs of gas accretion.

Another indicator of a galaxy's interaction and/or gas accretion history can come from disturbances to the gas distribution and kinematics. We make qualitative assessment of such disturbances from the CO position-velocity slices in Davis et al. (2013a) and from the CO integrated intensity maps and velocity fields in Alatalo et al. (2013a). Markers of disturbances include gas tails, strong asymmetries in the gas distribution, and complex velocity fields, and we thereby consider the following galaxies to have disturbed molecular gas: IC 1024, NGC 1222, NGC 3619, NGC 4150, NGC 4550, NGC 4694, NGC 4753, NGC 5173, NGC 7465, PGC 058114, and UGC 09519. These are the galaxies noted in Alatalo et al. (2013a) as classes 'M' (mildly disturbed) or 'X' (strongly disturbed), or which are sufficiently lopsided that their integrated CO spectrum from the CARMA data has a flux density twice as large on one side of the systemic velocity as on the other side. NGC 4550 is also noted by Crocker et al. (2009a) to have an asymmetric gas disc, based on observations from the IRAM Plateau de Bure interferometer. These classifications thus show disturbances in 11 of the 40 galaxies with CO maps. Additional possible cases of disturbed gas include NGC 2768 and NGC 3489 (Crocker et al. 2011). The qualitative assessments tend to be sensitive only to rather severe disruptions, and furthermore the sensitivity is undoubtedly nonuniform, but the classifications are adequate in these initial searches for large scale trends between disruptions and galaxy colour.

Kinematic disturbances are also evident in the atomic gas of many H I-rich galaxies, especially at several R_e and beyond (Serra et al. 2012, 2013). However, since that material at large radii does not appear to be associated with recent star formation activity within R_e (Section 4.2), we focus here on the kinematic information from the gas on kpc scales. The ATLAS^{3D} sample includes 15 galaxies with central HI detections from WSRT, but no CO map; of these 15, only one (NGC 7280) is identified as likely showing significant kinematically disturbed gas. We suspect that more candidates would be identified if the spatial resolution of the HI data were closer to that of the CO data.

The disturbance indicator provides a different perspective than the misalignment criterion discussed above, as it is useful even in cases with well-aligned stellar and gaseous angular momenta. It is also most sensitive to events within the last few orbital time-scales (typically a few $\times 10^7$ to 10^8 yr, Young 2002), and this may be the most appropriate time-scale for correlations with colour evolu-

tion. However, it may indicate tidal forces on pre-existing gas in a galaxy, rather than the accretion of new gas. Furthermore, as it is clearly dependent on the sensitivity and angular resolution of the images, we can at present only detect the most egregious disturbances. Deep optical images can help to distinguish between tidal interactions and gas accretion (Duc et al. 2011), and such work is ongoing, but for now we will take the disturbance indicator as a possible sign of accretion with these caveats.

6.2 Stellar populations vs. accretion/interaction signatures

Figure 9 shows an age-mass diagram again but with markers indicating the galaxies that have signs of gas accretion or gravitational interactions. There are significant overlaps between the indicators, so that many galaxies have two or three of the signs. The ATLAS^{3D} sample contains 158 galaxies with $\log(M_{\rm JAM}/M_\odot) \leqslant 10.7$, and 45 of them ($0.28 \pm 0.03$) are detected in CO emission or in central H I emission. We find that 21 of those 45 (0.47 ± 0.07) show misaligned gas, which we interpret as meaning they have accreted their gas from some external source. Further, 26 of them (0.58 ± 0.07) show misaligned gas and/or anomalously low stellar metallicities, and 28 of them (0.62 ± 0.07) show misaligned gas, low metallicities, and/or kinematic disturbances in the cold gas at radii $< R_e$. Thus, more than half of the low (stellar) mass, H_2-rich or H I-rich early-type galaxies appear to have accreted substantial amounts of cold gas. Considering the multiple markers of accretion and interaction makes a modest increase in this rate over considering misalignment alone. In contrast, only six of the 22 high stellar mass galaxies with central cold gas (0.27 ± 0.09) show any such signs.

From analysis of the stellar structures and kinematics, Cappellari et al. (2011b, 2013b) have suggested that fast rotator early-type galaxies are former spiral galaxies which have been quenched through some bulge growth processes (see also Cheung et al. 2012; Cappellari 2013). The fast rotators might conceivably retain some molecular gas through this transition. However, spirals almost always have kinematically aligned gas and stars (Bureau & Chung 2006, and references therein). We might thus expect that in the absence of a major merger or external accretion, quenched former spiral galaxies will have primarily aligned gas (like the red symbols in Figure 9) rather than strongly misaligned gas (blue symbols).

In this context, we consider whether the early-type galaxies with aligned gas might have had different evolutionary histories from those with misaligned gas. We restrict attention at this point to the low (stellar) mass galaxies, due to the small incidence of misaligned gas among massive galaxies. Statistical testing shows no compelling evidence that the low-mass, H I-rich and H_2-rich galaxies with misaligned gas differ from their counterparts with aligned gas. Specifically, Kolmogorov-Smirnov and Mann-Whitney U tests on the galaxy colours, equivalent SSP ages, metallicities, α-element abundances, stellar velocity dispersions, specific stellar angular momenta, and photometric disc-to-total light ratios give probabilities 0.13 to 0.99, none of which are small enough to infer a difference in the two populations. Ultimately the question may be decided through detailed exploration of the individual galaxies' star formation histories (McDermid et al. 2013), with deep optical imaging and measurements of the current star formation rates and gas depletion time-scales. At present we conclude that the cold gas in early-type galaxies includes some gas which may have been retained through the quenching transition to the red sequence, as well as some gas acquired in a major merger or accreted from an external source such as a satellite galaxy or the intergalactic medium. This suggestion is not new, of course (e.g. Thilker et al 2010). But for the first time we now bring statistical samples of cold gas kinematic data to compare with the stellar population and structural data.

Table 5. Misalignments and Disturbances in low-mass H_2-rich galaxies

	Relaxed CO	Disturbed CO	Total
aligned	21	6	27
misaligned	7	5	12
Total	28	11	39

Notes: UGC 05408 has such a poorly resolved CO distribution that it is not possible to classify as either relaxed or disturbed.

Kaviraj et al. (2012) have advocated the idea that all the dust and molecular gas in early-type galaxies is accreted from external sources, based on an analysis of dust lane galaxies in the Galaxy Zoo project. It is worth noting, however, that part of their argument is based on their sample's large inferred dust and molecular masses, $M(H_2)/M_\star \sim 0.013$. The dust detection rate in Kaviraj et al. (2012) is also substantially lower than our detection rate in CO (4% vs 22%). The dust lane galaxies identified in Kaviraj et al. (2012) thus represent only the extreme tail of H_2-rich early-type galaxies, and the current study probes further into the $M(H_2)/M_\star$ luminosity distribution.

Finally, in the context of reading the galaxies' histories it is also important to note that the kinematic disturbances we identify in the molecular gas may not be the result of accretion from some external source onto a gas-poor galaxy. Instead, they may be the result of a strong gravitational interaction on an already gas-rich early-type galaxy, or (in the case of lopsidedness) an internal instability. To test for these different possibilities, Table 5 gives the incidence of disturbances in the CO kinematics for the low-mass galaxies with both aligned and misaligned gas. We note that disturbances are somewhat more common among low-mass galaxies with misaligned gas ($5/12 = 0.42 \pm 0.14$) than among those with aligned gas ($6/27 = 0.22 \pm 0.08$). However, the Fisher exact and chi-squared contingency table tests do not give better than 95% confidence levels on rejecting the null hypothesis, so the sample sizes are still too small to associate disturbances preferentially with gas accretion (as opposed to outflow or tidal forces).

6.3 Models of accretion-driven colour and Hβ evolution

Extensive evidence for the accretion of cold gas, particularly in the low-mass 'blue tail' galaxies, raises additional questions about the colour evolution of early-type galaxies. For example, we may ask whether it is possible for a completely quiescent red sequence galaxy to become as blue as our observed blue galaxies, given the constraints of the observed molecular masses and star formation rates. Secondly, we may ask whether cold gas accretion onto a massive galaxy, with an associated burst of star formation, would necessarily drive the galaxy off the red sequence.

Here we explore these questions by constructing a set of toy models in which quiescent, red sequence galaxies of masses $\log(M_\star/M_\odot) = 10$ to 11.5 experience $3{\times}10^8$ $M_\odot$ of star formation activity at late times. Detailed information on the models is provided in the Appendix; briefly, we use the Flexible Stellar Population Synthesis codes of Conroy et al. (2010) to follow their colour and Hβ absorption line strength evolution through the star formation episode. The duration and strength of the 'blue tail' ex-

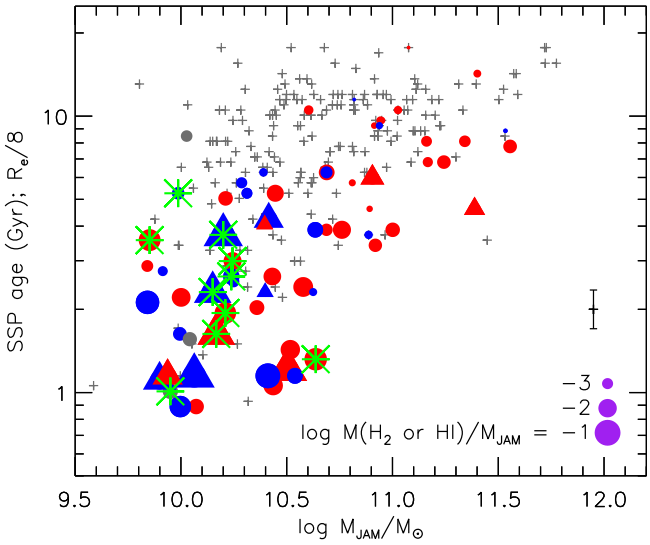

Figure 9. Similar to Figure 5, but here the circles and triangles indicate galaxies with either CO or central H I detections. Kinematically misaligned cold gas is indicated in blue and aligned (prograde) gas is in red. Galaxies showing significant disturbances in the molecular gas or H I (NGC 7280) are indicated with triangles and those showing relaxed gas are in circles. In all cases the symbol size indicates the scaled H_2 mass, if CO is detected, or the H I mass if CO is not detected. Outliers in the stellar mass-metallicity and mass-[α/Fe] relations are marked with green stars. The presence or absence of disturbances can only be noted for galaxies with CO or H I maps, and because only 70% of the CO detections are mapped we have only lower limits on the incidence of disturbances (triangles). For galaxies without CO maps we have used the kinematic misalignments measured in ionized gas or H I (Davis et al. 2011; Serra et al. 2013). NGC 0509, NGC 3073, and NGC 4283 are plotted in grey because they have insufficient kinematic information in all gas phases.

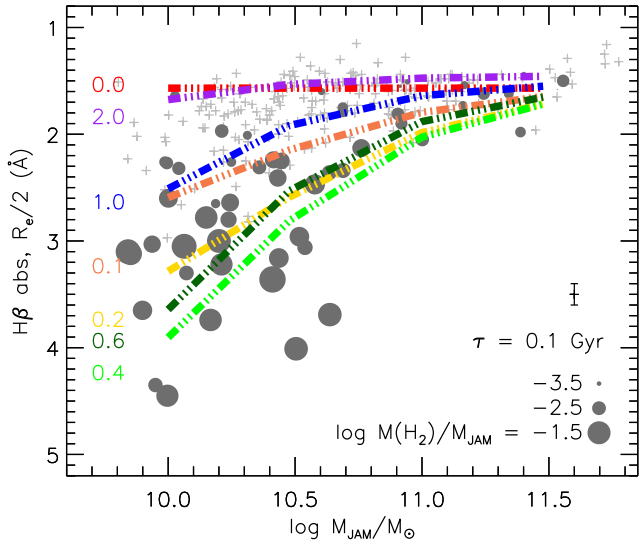

Figure 10. Similar to Figure 4, with overlays showing the evolution of old galaxies with 3×10^8 $M_\odot$ of recent star formation activity. The red line marked '0.0' shows the model red sequence before star formation is initiated, and subsequent lines show how Hβ changes through the late burst. Each isochrone is labelled with the time (in Gyr) since the initiation of the burst.

cursion is, of course, determined by the assumed mass of young stars and the time-scale over which the late star formation occurs. The mass of young stars in most ATLAS^{3D} galaxies is poorly constrained, but many of the blue tail galaxies have current molecular masses greater than 3×10^8 $M_\odot$, which at least lends plausibility to our assumption. In Fig 10 we show one example that follows the evolution of the Hβ absorption line strength through a burst of $\dot{M} \propto t\exp(-t/\tau)$, with $\tau = 0.1$ Gyr. The burst begins ($t = 0$) about 10 Gyr after most of the galaxy's stars formed, and the star formation rate peaks at a time $t = \tau$ and subsequently decays on a time-scale of τ. The Hβ line strength increases to a maximum of about 4Å for the lowest-mass galaxies and then, over a period of a couple Gyr, returns to its pre-burst value. In a similar spirit, Scott et al. (2013) have shown that ATLAS^{3D} galaxies with young central populations and low central Mg b values will return to the nominal Mg b–V_{esc} relation after several Gyr of passive evolution. The behaviors for other time-scales and for $u - r$ and NUV−K colours are also shown in the Appendix.

The toy models clearly show that it is plausible to explain the blue tail galaxies as former red sequence galaxies, with a quantity of recent star formation which is consistent with the observed H_2 masses in the ATLAS^{3D} sample. The required star formation rates are also consistent with those observed (Crocker et al. 2011; Shapiro et al. 2010, Appendix A). In this excursion scenario relatively short star formation time-scales, $\tau \sim 0.1$ to 0.3 Gyr, are required in order to reproduce the bluest galaxies with the strongest Hβ absorption. For the massive galaxies, a tight red sequence (particularly in NUV−K) favors longer star formation time-scales or older bursts, as discussed in more detail in the Appendix. Detailed studies of the galaxies' star formation histories are necessary for moving beyond this very simple plausibility check, but the models are consistent with a picture in which gas accretion onto red sequence galaxies could produce at least some of the blue tail galaxies.

Galaxy mergers are often associated with enhanced star formation activity, as in the case of the luminous and ultraluminous IR galaxies (LIRGs and ULIRGs); the mechanism is thought to be the galaxy-scale shocks driving the molecular gas to higher densities. In this context it is interesting to pursue the question of whether the galaxies with kinematic signs of gas accretion or disturbance have shorter star formation time-scales than the galaxies with quiescent kinematics. As noted above, such differences are not measurable in integrated colours or the $R_e/2$ Hβ absorption strengths. Davis et al. (2013b) also find that such differences are not obvious in star formation rates measured from mid-IR emission.

Some recent studies of the galaxy colour-magnitude diagram (e.g. Gonçalves et al. 2012) have assumed that galaxies in the 'green valley' are exclusively becoming redder, on the approach to the red sequence. At face value, such an assumption would seem to be in direct contradiction of the toy model employed here. However, our toy model does apply to a somewhat special population of galaxies, the H_2-rich early-type galaxies. In addition, their movement through the green valley is faster on the blueward track than on the return redward track, so even in the context of this 'excursion' model there will be a greater proportion of galaxies moving redward than moving blueward.

7 HIGH-MASS VS. LOW-MASS GALAXIES

Section 6 discusses evidence that the cold gas in low-mass early-type galaxies is commonly accreted. However, the picture is much less clear for the high-mass H_2-rich galaxies, since their incidence of disturbed or misaligned gas is lower. The detectability of kinematic misalignments and other gas disturbances should not depend on the stellar mass of the galaxy, except to the extent that the disturbed cold gas will evolve on an orbital time-scale towards circular orbits in a stable plane. In our mostly oblate gas-rich galaxies, the evolution will be towards prograde or retrograde orbits in the equatorial plane, and the orbital time-scales are shorter for a larger galaxy mass (at fixed radius). Thus the difference in the rates of misalignment or gas disturbance between low-mass and high-mass galaxies is probably real, though it may simply mean that the high-mass galaxies accreted their gas in the more distant past. For further discussion, see Davis et al. (2011) and Sarzi et al. (2006). On the other hand, the metallicity signatures of accreted gas should be more easily distinguished in a smaller host stellar population. The catalog of low-metallicity accreted gas is expected to be strongly incomplete for large stellar masses.

In a study of the hot gas in ATLAS^{3D} galaxies, Sarzi et al. (2013) note that interactions between hot and cold gas may have a significant effect on the cold gas. They propose that the higher mass fast rotators, due to their deeper gravitational potentials, may have recycled more of their internal stellar mass loss into a hot ISM. This recycled gas would necessarily be kinematically aligned with the stellar rotation, and it might shock heat any incoming misaligned gas (thus producing the lack of misaligned molecular gas in high-mass galaxies). Bogdán et al. (2012) have also presented a case study of the hot gas content of four high-luminosity ($M_K \sim -24.0$) ATLAS^{3D} galaxies, and they demonstrate that early-type galaxies of similar optical luminosity can have hot gas of very different distributions and kinematic states. A proper treatment of the interaction of hot gas and cold gas should take into account the possible angular momentum transfer between the gas phases.

We have commented several times that there is a striking difference in the SSP age and Hβ absorption line strength scatter of high and low-mass early-type galaxies. Scott et al. (2013) have also made the same comment about the Mg b line strengths and escape velocities in the ATLAS^{3D} sample. In colour and Hβ, some of this difference is due to the relative gas masses; specifically, the high-mass galaxies tend to have smaller $M(H_2)/M_{JAM}$ ratios. However, as Figure 11 shows, there is a significant range of overlap and values of $M(H_2)/M_\star$ from $10^{-2.4}$ to 10^{-4} can be found in both high-mass and low-mass early-type galaxies. Under the very simplistic assumption that a fixed $M(H_2)/M_\star$ corresponds to a fixed percentage of young stars in a late starburst, one might then expect all galaxies of the same $M(H_2)/M_\star$ to have the same SSP age. Instead, we observe that high-mass galaxies have systematically larger SSP ages even at the *same* values of $M(H_2)/M_\star$ or $M(H_2)/M_{JAM}$ as low-mass galaxies. The trend suggests differences in the star formation efficiencies and/or the accretion and star formation histories between low-mass and high-mass galaxies. Naab et al. (2013) discuss the star formation and assembly histories of simulated high-mass and low-mass early-type galaxies, for example, and note that the high-mass galaxies have older stellar populations. The differences might also be related to the fact that the high-mass galaxies tend to have kinematically quiescent, prograde gas, so presumably they have fewer internal shocks to drive enhanced star formation.

In addition, the morphological quenching mechanism studied by Kawata et al. (2007) and Martig et al. (2013) (among others) might explain this trend, as it invokes greater local stability of the gas in a deeper and steeper gravitational potential. For example, Martig et al. (2013) make high-resolution simulations of a cold gas disc (7.5×10^8 $M_\odot$) in a galaxy with $M_\star = 5.6 \times 10^{10}$ $M_\odot$; this galaxy then has $M(H_2)/M_\star \sim 0.013$, similar to the most H_2-rich of our high-mass early-type galaxies. If the galaxy's stellar mass distribution is spherical, they find the cold gas only reaches maximum densities of 600 cm^{-3}, whereas if the stellar distribution is flattened like a spiral, the cold gas reaches 4×10^5 cm^{-3}. This difference suggests the same gas will have substantially longer depletion time-scales in a spherical galaxy than in a flat galaxy. For specific application to the ATLAS^{3D} sample, we note that Cappellari et al. (2013b) have demonstrated that the high-mass early-type galaxies tend to be spheroid-dominated whereas the low-mass galaxies include both spheroid-dominated and disc-dominated systems. One remaining question is whether this kind of a quenching mechanism by itself can explain the apparent sharp and dramatic increase in colour dispersion at low masses or whether, as mentioned above, some systematic difference in gas accretion histories is also required. These issues can be addressed in more detail by comparing the star formation histories and current gas depletion time-scales of ATLAS^{3D} galaxies.

There are several other differences between the dust and ISM properties of high-mass and low-mass early-type galaxies. di Serego Alighieri et al. (2013) find that higher mass Virgo Cluster early types tend to have higher dust temperatures than their counterparts at lower stellar mass. The reason for the trend is not yet known. Crocker et al. (2012) have also noted correlations between stellar mass and the physical properties of the molecular gas in ATLAS^{3D} galaxies. The high-mass galaxies tend to have larger $^{13}CO/^{12}CO$ ratios and larger $HCN/^{12}CO$ ratios. The proposed interpretation of these trends is that they are driven by the kinematic state of the gas (as noted above, the high-mass galaxies are less likely to have disturbed or misaligned molecular gas). But the physical properties of the molecular gas both affect, and are affected by, star formation activity, and with the existing data it is still diffi-

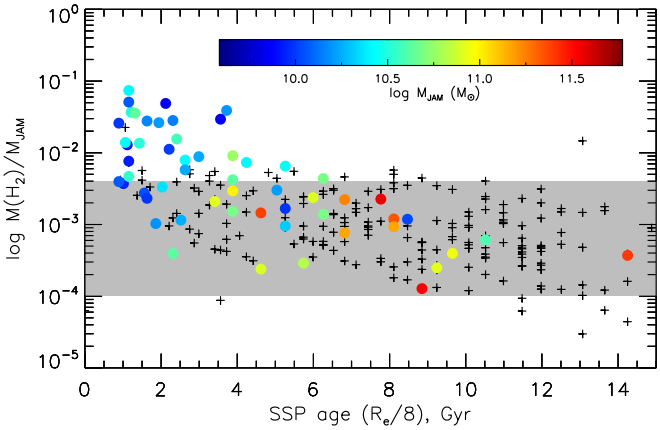

Figure 11. Molecular gas content vs. SSP age; crosses are CO nondetections, and colour circles are CO detections. The colour of each circle indicates the total stellar mass $\log(M_{JAM}/M_\odot)$ as noted in the colourbar. As expected, there is a general trend such that galaxies with larger molecular contents tend to have younger stellar ages. In addition, for $M(H_2)/M_{JAM}$ in the range $10^{-2.4}$ to 10^{-4} (gray box), galaxies of larger stellar mass M_{JAM} have systematically larger SSP ages even though they have the same molecular gas content (normalized to stellar mass).

cult to disentangle these causal relationships from environmental effects such as stripping in clusters and groups. Additional work on the details of the molecular gas properties would be valuable for understanding the star formation efficiencies of early-type galaxies.

8 SUMMARY

We present a study of the relationships between the cold gas (H I and H_2) content of early-type galaxies and their stellar populations, as encoded in Hβ absorption line strengths, $u-r$ and NUV$-$K colours. Detection rates of H I and H_2 are $\geqslant 50\%$ in 'blue tail' early-type galaxies, depending somewhat on how the blue tail is defined. Similarly, the low-mass H_2-rich early-type galaxies are usually more blue and have younger stellar populations than their H_2-poor counterparts, especially when measured in Hβ absorption and NUV$-$K colours, and less frequently at $u-r$.

Detection rates of H I and H_2 are also nonzero for red sequence early-type galaxies, *no matter how the red sequence is defined*. These detection rates range from 10% to 30% for galaxies with masses $\log(M_{\rm JAM}/M_\odot) = 9.8$ to 11.8 and for different definitons of the red sequence. The result is at least qualitatively consistent with the detection rates of dust in red sequence early-type galaxies (e.g. Smith et al. 2012). The red sequence thus contains high mass early-type galaxies with abundant cold gas; specifically, with H_2 masses up to 8×10^8 $\mathrm{M}_\odot$ and H I masses up to 4×10^9 $\mathrm{M}_\odot$. These results may serve as a reminder that 'photometric gas fractions' are merely averages over the relevant populations, and individual galaxies can deviate strongly from those averages. Colour corrections for the reddening associated with the molecular gas and dust do not materially alter these conclusions.

The H_2-rich and H I-rich massive early-type galaxies have the same median colour and same colour dispersion as their analogs without cold gas. To first order, the reason for this behavior is straightforward. The massive galaxies tend to have smaller $\mathrm{M_{gas}/M_\star}$, so they probably also have smaller ratios $\mathrm{M_{new}/M_{old}}$ (where $\mathrm{M_{new}}$ is the mass of young stars and $\mathrm{M_{old}}$ is the mass of old stars). The young stellar populations will therefore be more difficult to detect via their colour effects on a large host galaxy.

However, $\mathrm{M_{gas}/M_\star}$, or even M(H_2)/$\mathrm{M_\star}$, does not uniquely predict the colour and mean stellar age of an early-type galaxy; we note that massive galaxies have older stellar populations than low-mass galaxies *even at the same values of* $\mathrm{M_{gas}/M_\star}$. We speculate that the low-mass galaxies may have shorter gas depletion time-scales or that they may have acquired their cold gas more recently. Additional high sensitivity, high resolution molecular and radio continuum observations (such as are now available with ALMA and the JVLA) will complement improved simulations (e.g. Martig et al. 2013) in addressing these questions.

Atomic gas in early-type galaxies is not as closely related to star formation activity as molecular gas is. Many H I-rich early-type galaxies are still on the red sequence, at all stellar masses and in all indicators of colour, Hβ absorption and SSP age. That result is largely driven by the differing spatial scales of the measurements. Specifically, the stellar population indicators we are working with here are dominated by stars within an effective radius or less, but much of the H I is at several R_e and beyond (Serra et al. 2012). At the moment we are not considering young stellar populations in extended UV rings. Furthermore, *if* the large-scale H I distributions were serving as reservoirs of cold gas to drive star formation activity in the cores of their galaxies, we might expect total H I content to correlate with colour, Hβ strength or SSP age in the same sense that the H_2 mass does. But this correlation is not observed in the extended H I, only in the central H I. The time-scales over which the extended H I can serve as a reservoir may be too long for us to notice the correlation; or we might be finding these extended H I systems in a stage prior to conversion of H I into H_2 and star formation activity.

These relationships between cold gas content, galaxy colour, and Hβ absorption can produce selection biases in samples of red sequence galaxies. For example, the detection rates of cold gas are larger among the massive red sequence galaxies than the low-mass red sequence galaxies.

We have also analyzed the stellar properties of galaxies with and without signs that their cold gas was accreted from some external source. These signs include kinematic misalignments between gas and stars, disturbed gas kinematics, and departures from the stellar mass-metallicity relation. As Davis et al. (2011) have already commented, kinematic misalignments are not common at high stellar masses or among the Virgo Cluster members, so we infer that $\sim 20\%$ of the high-mass early-type galaxies galaxies may have retained or recycled their cold interstellar medium. However, at low stellar masses, $\sim 60\%$ of the H I- and H_2-rich galaxies show at least one of the signs that the cold gas was accreted.

Simple toy models can explain the colours and Hβ absorption strengths of the H_2-rich ATLAS^{3D} galaxies in a "frosting" or rejuvenation scenario. Even the bluest of them could be formerly quiescent, red sequence galaxies which acquired a modest amount of cold gas and recent star formation. The required star formation rates and gas masses are broadly consistent with those observed. Of course, this colour analysis provides only a plausibility argument for the rejuvenation scenario and more detailed work on the galaxies' star formation histories is necessary.

We have searched for significant structural or stellar population differences between the gas-rich galaxies that clearly show signs of external accretion, and the gas-rich galaxies with relaxed, kinematically aligned gas. No notable differences are found. But some of the prograde, well-aligned cold gas may also have been accreted, and additional theoretical work on the expected angular momentum distributions of accreted material would be valuable.

Some of the implications of this work include the idea that red sequence galaxies should not be assumed to be free of cold gas, even if a morphological cut is made to exclude red spirals and retain only red early-type galaxies. Early-type galaxies in the green valley may have recently acquired cold gas, and may still be becoming bluer. Furthermore, for galaxies of $\log(M_{\rm JAM}/M_\odot) > 10.7$ and cold gas masses up to a few 10^9 $\mathrm{M}_\odot$, and for the sample size we have here, the presence of H_2 and H I do not measurably affect integrated colours, the red sequence ridgeline or its colour dispersion. Hence, within these parameters, great care must be taken to make inferences about the cold gas content and star formation rates of galaxies from the colour evolution of the red sequence or the lack of such evolution.

ACKNOWLEDGMENTS

This research was partially supported by grant NSF-1109803 to LMY. Thanks also to Dr. Paul T. P. Ho for the invitation to spend a sabbatical at ASIAA. MC acknowledges support from a Royal Society University Research Fellowship. This work was supported by the rolling grants Astrophysics at Oxford PP/E001114/1 and ST/H002456/1 and visitors grants PPA/V/S/2002/00553, PP/E001564/1 and ST/H504862/1 from the UK Research Coun-

cils. RLD acknowledges travel and computer grants from Christ Church, Oxford and support from the Royal Society in the form of a Wolfson Merit Award 502011.K502/jd. RLD is also grateful for support from the Australian Astronomical Observatory Distinguished Visitors programme, the ARC Centre of Excellence for All Sky Astrophysics, and the University of Sydney during a sabbatical visit. SK acknowledges support from the Royal Society Joint Projects Grant JP0869822. RMcD is supported by the Gemini Observatory, which is operated by the Association of Universities for Research in Astronomy, Inc., on behalf of the international Gemini partnership of Argentina, Australia, Brazil, Canada, Chile, the United Kingdom, and the United States of America. TN and MBois acknowledge support from the DFG Cluster of Excellence 'Origin and Structure of the Universe'. MS acknowledges support from a STFC Advanced Fellowship ST/F009186/1. PS acknowledges support of a NWO/Veni grant. (TAD) The research leading to these results has received funding from the European Community's Seventh Framework Programme (/FP7/2007-2013/) under grant agreement No 229517. MBois has received, during this research, funding from the European Research Council under the Advanced Grant Program Num 267399-Momentum. The authors acknowledge financial support from ESO.

Funding for SDSS-III has been provided by the Alfred P. Sloan Foundation, the Participating Institutions, the National Science Foundation, and the U.S. Department of Energy Office of Science. The SDSS-III web site is http://www.sdss3.org/.

SDSS-III is managed by the Astrophysical Research Consortium for the Participating Institutions of the SDSS-III Collaboration including the University of Arizona, the Brazilian Participation Group, Brookhaven National Laboratory, University of Cambridge, Carnegie Mellon University, University of Florida, the French Participation Group, the German Participation Group, Harvard University, the Instituto de Astrofisica de Canarias, the Michigan State/Notre Dame/JINA Participation Group, Johns Hopkins University, Lawrence Berkeley National Laboratory, Max Planck Institute for Astrophysics, Max Planck Institute for Extraterrestrial Physics, New Mexico State University, New York University, Ohio State University, Pennsylvania State University, University of Portsmouth, Princeton University, the Spanish Participation Group, University of Tokyo, University of Utah, Vanderbilt University, University of Virginia, University of Washington, and Yale University.

REFERENCES

Aihara H., Allende Prieto C., An D., et al., 2011, ApJS, 193, 29
Alatalo K., Davis T. A., Bureau M., et al., 2013, MNRAS, 432, 1796
Alatalo K., Nyland K., et al., 2013, ApJ, submitted
Auld R., Bianchi S., Smith M. W. L., et al., 2013, MNRAS, 428, 1880
Bacon R., Copin Y., Monnet G., et cl., 2001, MNRAS, 326, 23
Bell E., et al., 2003, ApJS, 149, 289
Binney J., Tremaine S. 2008, Galactic Dynamics, 2nd ed. (Princeton, NJ: Princeton University Press)
Blanton M., Kazin E., Muna D., et al., 2011, AJ, 142, 31
Bois M., et al., 2011, MNRAS, 416, 1654 (Paper VI)
Bogdán Á., David L. P., Jones C., Forman W. R., & Kraft R. P., ApJ, 758, 65
Blitz L., Rosolowsky E., 2006, ApJ, 650, 933
Bureau M., Chung A., 2006, MNRAS, 366, 182
Cappellari M., et al., 2011, MNRAS, 413, 813 (Paper I)
Cappellari M., et al., 2011, MNRAS, 416, 1680 (Paper VII)
Cappellari M., Scott N., et al., 2013, MNRAS, 432, 1709
Cappellari M., McDermid R. M., et al., 2013, MNRAS, 432, 1862
Cappellari M., 2013, ApJ, 778, 2
Carter D., Pass S., Kennedy J., Karick A. M, Smith R. J., 2011, MNRAS, 414, 3410
Cheung E., Faber S. M., Koo D. C., et al., 2012, ApJ, 760, 131
Chou R. C. Y., Bridge C. R., Abraham R. G., 2012, ApJ, 760, 113
Conroy C., Gunn J. E., 2010, ApJ, 712, 833
Cortese L., Gavazzi G., & Boselli A. 2008, MNRAS, 390, 1282
Cortese L., Hughes T. M., 2009, MNRAS, 400, 1225
Crocker A. F., Jeong H., Komugi S., et al., 2009, MNRAS, 393, 1255
Crocker A. F., Bureau M., Young L. M., Combes F., 2008, MNRAS, 386, 1811
Crocker A. F., Bureau M., Young L. M., Combes F., 2011, MNRAS, 410, 1197
Crocker A. F., Krips M., Bureau M., et al., 2012, MNRAS, 421, 1298
Crockett R. M., Kaviraj S., Silk J. I., et al., 2011, ApJ, 727, 115
Davis T. A., Alatalo K., Sarzi M., et al. 2011, MNRAS, 417, 882
Davis T. A., Bureau M., et al. 2013, MNRAS, 429, 534
Davis T. A., ATLAS^{3D} team, in preparation
de Zeeuw P. T., et al., 2002, MNRAS, 329, 513
di Serego Alighieri S., Bianchi S., Papplardo C., et al., 2013, A&A, 552, 8
Donas J., Deharveng J.-M., Rich R. M., et al. 2007, ApJS, 173, 597
Duc P.-A., Cuillandre J.-C., Serra P., et al. 2011, MNRAS, 417, 863
Emsellem E., et al., 2011, MNRAS, 414, 888
Fumagalli M., Labbe I., Patel S. G., et al., 2013, ApJ, submitted (arXiv:1308.4132)
Gil de Paz A., Boissier S., Madore B. F., et al. 2007, ApJS, 173, 185
Gonçalves T. S., Martin D. C., Menéndez-Delmestre K., Wyder T. K., & Koekemoer A., 2012, ApJ, 759, 67
Goudfrooij P., de Jong T., 1995, A&A, 298, 784
Jaffé Y. L., Aragón-Salamanca A., De Lucia G., et al., 2011, MNRAS, 410, 280
Jarrett T. H., Chester T., Cutri R., Schneider S., Skrutskie M., Huchra J. P., 2000, AJ, 119, 2498
Jeong H., Yi S. K., Bureau M., Davies R. L., et al. 2009, MNRAS, 398, 2028
Johnson B. D., Schiminovich D., Seibert M., et al., 2007, ApJS, 173, 392
Kauffmann G., Li C., Fu J., et al. 2012, MNRAS, 422, 997
Kaviraj S., Schawinski K., Devriendt J. E. G., et al. 2007, ApJS, 173, 619
Kaviraj S., Schawinski K., Silk J., Shabala S. S., 2011, MNRAS, 415, 3798
Kaviraj S., Ting Y-S., Bureau M., et al., 2012, MNRAS, 423, 49
Kawata D., Cen R., Ho L. C. 2007, ApJ, 669, 232
Khochfar S., et al., 2011, MNRAS, 417, 845
Krajnović D., et al., 2011, MNRAS, 414, 2923
Krajnović D., et al., 2013, MNRAS, 432, 1768
Kuntschner H., et al., 2010, MNRAS, 408, 97
Leroy A., Walter F., Brinks E., et al. 2008, AJ, 136, 2782
Lucero D. M., Young L. M., 2013, AJ, 145, 56
Martig M., Bournaud F., Teyssier R., Dekel A., 2009, ApJ, 707, 250

Martig M., Crocker A. F., Bournaud F., et al., 2013, MNRAS, 432, 1914
Martini P., Dicken D., & Storchi-Bergmann T., 2013, ApJ, 766, 121
McDermid R. M., ATLAS^{3D} team, in preparation
Morganti R., de Zeeuw P. T., Oosterloo T. A., et al., 2006, MNRAS, 371, 157
Naab T., Oser L., Emsellem E., et al., 2013, MNRAS, in press (arXiv:1311.0284)
Ogle P., Boulanger F., Guillard P., et al., 2010, ApJ, 724, 1193
Oosterloo T., Morganti R., Crocker A., et al., 2010, MNRAS, 409, 500
Saintonge A., Kauffmann G., Kramer C., et al., 2011, MNRAS, 415, 32
Saintonge A., Tacconi L. J., Fabello S., et al., 2012, ApJ, 758, 73
Sarzi M., et al., 2006, MNRAS, 366, 1151
Sarzi M., et al., 2010, MNRAS, 402, 2187
Sarzi M., et al., 2013, MNRAS, 432, 1845
Schiminovich D., Wyder, T. K., Martin, D. C., et al. 2007, ApJS, 173, 315
Schlafly, E. F., & Finkbeiner, D. P. 2011, ApJ, 737, 103
Schlegel D. J., Finkbeiner D. P., Davis M. 1998, ApJ, 500, 525
Scott N., Cappellari M., Davies R. L., et al., MNRAS, 432, 1894
Serra P., Trager S. C., MNRAS, 374, 769
Serra P., Trager S. C., Oosterloo T. A., Morganti R., 2008, A&A, 483, 57
Serra P., et al., 2012, MNRAS, 422, 1835
Serra P., Oser L., Krajnović D., et al., 2013, MNRAS, submitted
Shapiro K. L., Falcón-Barroso J., van de Ven G., et al. 2010, MNRAS, 402, 2140
Smith M. W. L. et al., 2012, ApJ, 748, 123
Snyder G., Brodwin M., Mancone C. M., et al., 2012, ApJ, 756, 114
Suh H., Jeong H., Oh K., et al., 2010, ApJS, 187, 374
Thilker D. A., Bianchi L., Schiminovich D., et al., 2010, ApJ, 714, 171
Trager S., Faber S. M., Worthey G., González J. J., 2000, AJ, 120, 165
Wei L. H., Vogel S. N., Kannappan S. J., Baker A. J., Stark D. V., Laine S., 2010, ApJL, 725, L62
Weijmans A.-M., et al., 2013, MNRAS, submitted
Welch G. A., Sage L. J., Young L. M., 2010, ApJ, 725, 100
Wyder, T. K., Martin, D. C., Schiminovich, D., et al., 2007, ApJS, 173, 293
Yi S. K., et al., 2005, ApJL, 619, L111
Young L. M., 2002, AJ, 124, 788
Young L. M., 2005, AJ, 634, 258
Young L. M., Bureau, M., & Cappellari, M. 2008, ApJ, 676, 317
Young L. M., Bendo G., Lucero D. M. 2009, AJ, 137, 3053
Young L. M., et al. 2011, MNRAS, 414, 940

APPENDIX A: TOY MODELS FOR COLOUR AND Hβ EVOLUTION

We make a quantitative assessment of the effects of recent star formation on red sequence galaxies using the Flexible Stellar Population Synthesis codes (version 2.4) of Conroy et al. (2010). Specifically, we model a scenario in which a relatively small amount of cold molecular gas drops into a red sequence galaxy and ignites star formation (Cortese & Hughes 2009; Kaviraj et al. 2011), and we follow the colour and Hβ evolution of these simple models. We use the Padova isochrones and a Chabrier initial mass function. For following integrated colours, the BaSeL spectral library is used because it has a larger wavelength coverage than MILES; but for Hβ absorption, the MILES spectral library is used as it has the best match to the ATLAS^{3D} optical spectroscopic resolution. The evolution is traced by first constructing models of old, red sequence galaxies with ages of 8.5 to 10.3 Gyr, metallicities [Fe/H] of solar to +0.2 dex, and stellar masses appropriate to span the range of luminosities in the ATLAS^{3D} sample. The ages and metallicities of this old population are adjusted by hand to reproduce the slope of the red sequence, but that is purely for cosmetic purposes and we do not attempt to infer anything about the details of the old stellar populations in this analysis. The Hβ "red sequence" is a simpler solar metallicity model with an age of 10.2 Gyr. Late bursts of star formation are then superposed, and the evolution of the composite population is followed to produce "red sequence" isochrones following the burst. No extinction is assumed on the young population, so the colour isochrones illustrate the limiting case of the maximum excursion from the red sequence.

The total mass of stars formed in the late burst is always $\int \dot{M} dt = 3 \times 10^8$ M$_\odot$, motivated by the fact that the largest molecular masses inferred in the ATLAS^{3D} sample are on the order of 3×10^9 M$_\odot$. A stellar mass of 3×10^8 M$_\odot$ is therefore reasonable in the sense that it is smaller than many of the currently known molecular masses. Interestingly, an HST study of NGC 4150 (one of our low-mass blue tail galaxies) infers that it contains 1–2×10^8 M$_\odot$ of young stars (Crockett et al. 2011), though its current molecular mass is only 7×10^7 M$_\odot$ (Young et al. 2011). In short, the mass of young stars can also be larger than the current molecular mass if a significant portion of that gas has already been consumed or destroyed. The use of a constant mass of young stars, independent of total stellar luminosity, is also motivated by the statistical work in Paper IV showing that the M(H_2) distributions are independent of stellar luminosity.

Four sets of models are produced for different star formation histories in the late burst; one set assumes an instantaneous burst, and three are delayed τ models with $\dot{M}(t) \propto te^{-t/\tau}$ for $\tau = 100$ Myr, 300 Myr, and 1 Gyr. In this assumed form, the star formation rate peaks at time $t = \tau$, so that τ describes the time-scale for the initial ramp-up of the star formation rate from zero to its peak as well as for the decay from the peak back down to zero. The instantaneous burst ($\tau = 0$) is clearly unphysical; even in the case of an extreme violent merger one would still expect gas to fall in on a dynamical time-scale, but the model is presented for context. The exponential cutoff in the star formation rate is imposed so that the models will gradually return to the red sequence. In the real universe such a cutoff might be driven by consumption of the cold gas, by its destruction or expulsion in AGN-driven feedback, or something else, but we are agnostic about the cause of the cutoff and merely observe its effects on the stellar population.

The peak star formation rates in the delayed τ models are 1.1 M$_\odot$ yr^{-1}, 0.37 M$_\odot$ yr^{-1}, and 0.11 M$_\odot$ yr^{-1}. In these models the star formation rate is within 90% of its peak value for the time period 0.6τ to 1.5τ and is significantly lower outside that time range. For comparison, the star formation rates inferred for the ATLAS^{3D} galaxies by Shapiro et al. (2010), Crocker et al. (2011), and Davis et al. (2013b) from observations of PAH, 22μm, 24μm and FUV emission are 0.006 to 3 M$_\odot$ yr^{-1} and gas consumption time-scales fall in the range 0.1 Gyr to 4 Gyr. Wei et al (2010) also measured gas consumption time-scales in a different set of early-type galaxies to be 0.3 to 10 Gyr. Thus the delayed τ models are consistent with observed star formation rates.

Figures A1 to A3 show the $u - r$, NUV$-$K, and Hβ line strength models compared to the ATLAS^{3D} galaxies *after* correction for internal extinction. As expected, the models all show an excursion off the red sequence to bluer colours or stronger Hβ absorption, followed by a gradual return to the red sequence as star formation activity decreases. For a fixed quantity of star formation, less massive galaxies make larger excursions. Spreading out the star formation over a longer time-scale produces weaker excursions but with longer durations. In addition, the NUV$-$K colours are the most sensitive to the current star formation rate. The Hβ absorption line strength has a delayed response to star formation as it is dominated by the A stars; Hβ always reaches its maximum a few hundred Myr after $u - r$ and NUV$-$K have passed their minima.

The slow star formation models ($\tau = 1$ Gyr, or peak SFR $<$ 0.1 $\mathrm{M}_{\odot}$ yr^{-1}) do not become blue enough, particularly in $u-r$ and Hβ absorption, to explain the observed H_2-rich blue tail galaxies. Models with faster bursts can easily explain the blue tail galaxies; on the other hand, such models exhibit much larger ranges of NUV$-$K colours than do the high-mass ATLAS^{3D} galaxies. Thus, in the context of these excursion models it is nontrivial to explain simultaneously the tightness of the red sequence at high masses and the numbers of blue galaxies at low masses. In order to reproduce these effects with the simple toy models, we would be driven to three possible interpretations: *(i)* that the high-mass galaxies favor longer star formation time-scales and lower star formation efficiencies than the low-mass galaxies; *(ii)* that the high-mass galaxies had their late burst systematically longer in the past; and/or *(iii)* that the excursion model does not apply to both high-mass and low-mass galaxies, as perhaps the low-mass galaxies have never yet been up to the red sequence. More detailed investigations of the galaxies' star formation histories should help to distinguish between these possibilities.

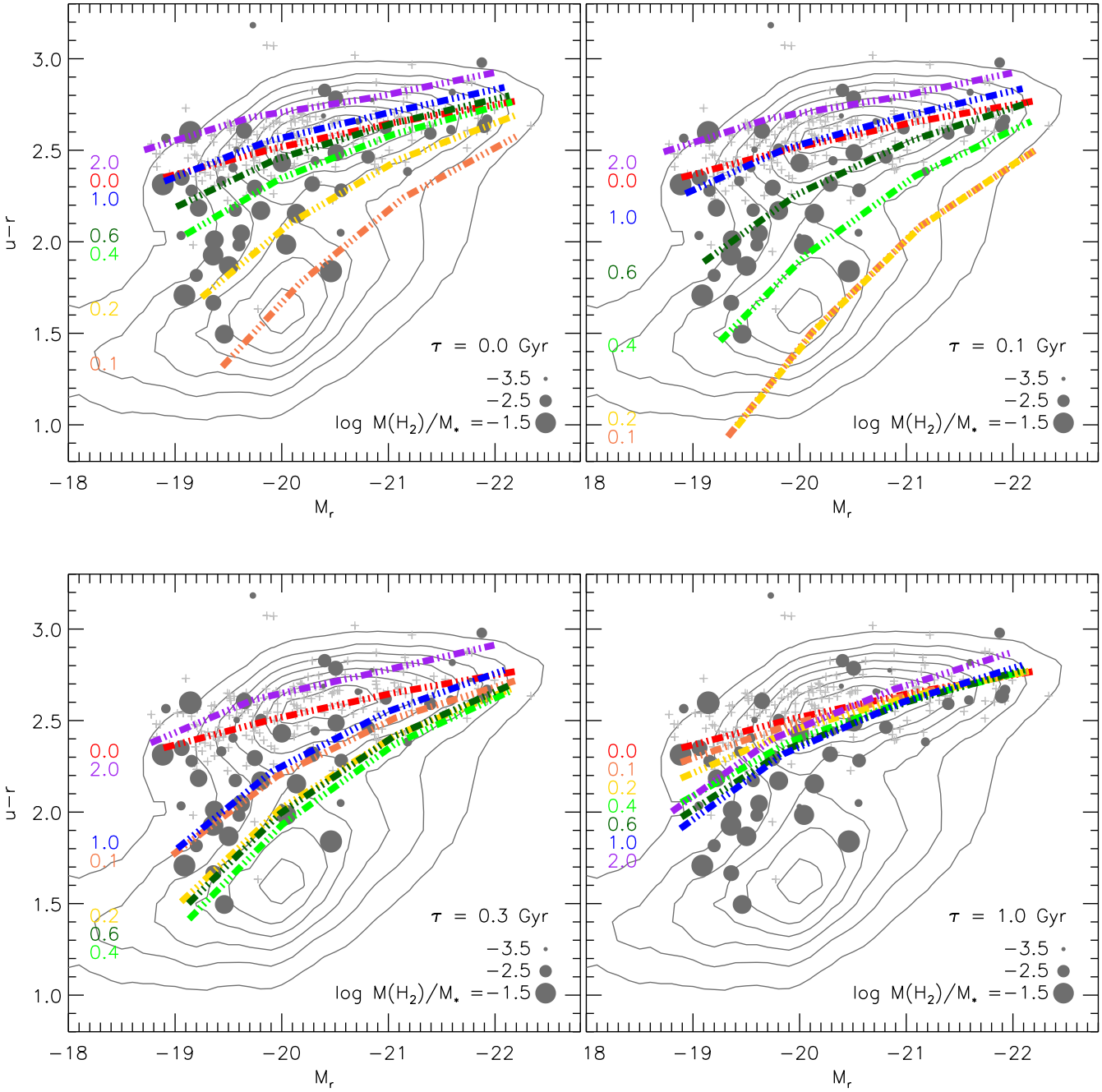

Figure A1. Model isochrones for a simple scenario in which cold gas drops onto a red sequence galaxy and initiates some star formation activity. The total mass of stars formed is 3×10^8 $M_\odot$. Panels show four different star formation histories for the late burst, including a delta function ($\tau = 0$ Gyr) and delayed tau models with $\tau = 100$ Myr, 300 Myr, and 1 Gyr. Dashed lines indicate the location of the "red sequence" at the times indicated (in Gyr, relative to the beginning of the burst). Contours and other symbols are the same as in Figure 7, with the exception that here the symbol size is the normalized H_2 mass. In the $\tau = 0$ panel, an isochrone earlier than 0.1 Gyr would show yet bluer colours; in the other panels, the minimum in $u - r$ colours can be seen where the isochrones change from becoming bluer with time to becoming redder.

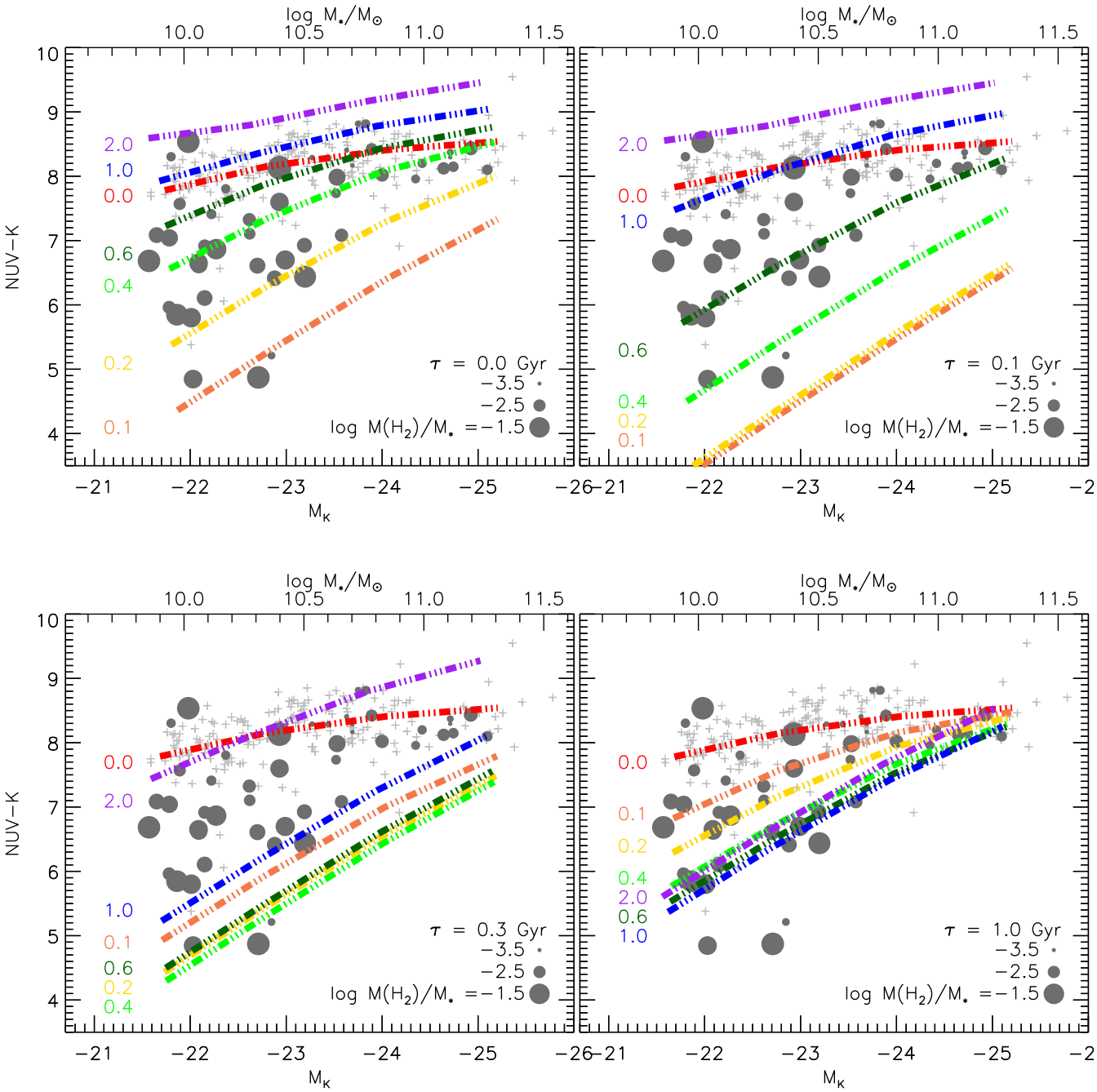

Figure A2. Similar to Figure 8, with NUV−K model isochrones.

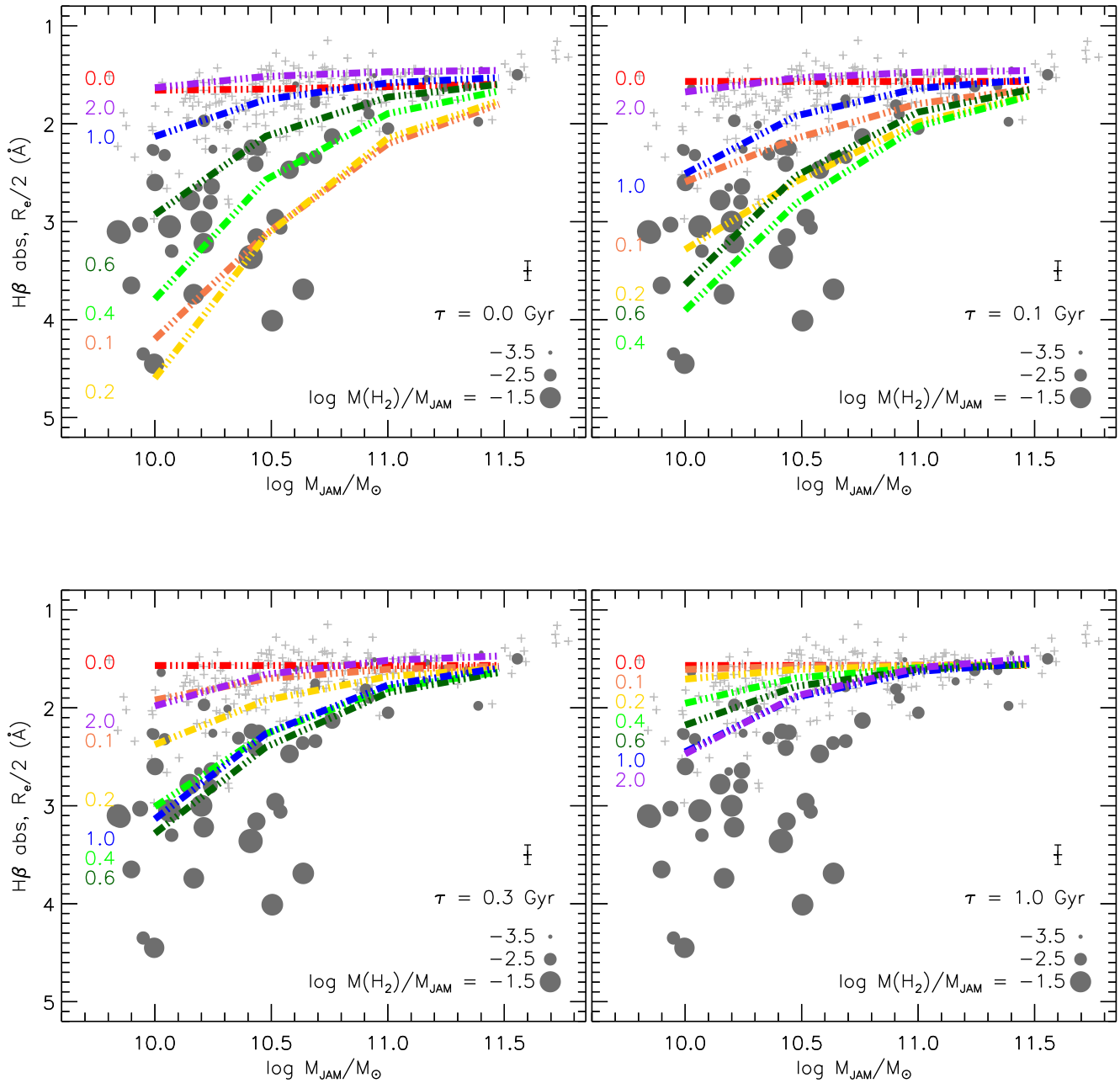

Figure A3. Hβ-mass diagram, similar to Figure 4, with model isochrones.